Planet. Space Sci., Vol. 25, pp. 243 to 260. Pergamon Press, 1977. Printed in Northern Ireland

# AURORAL ION VELOCITY DISTRIBUTIONS FOR A POLARIZATION COLLISION MODEL

J.-P. ST-MAURICE
Department of Atmospheric and Oceanic Science, The University of Michigan, Ann Arbor, MI 48109, U.S.A.

and

R. W. SCHUNK*
Department of Applied Physics and Information Science, University of California at San Diego, La Jolla, CA 92093, U.S.A.

(*Received in final form* 19 *August* 1976)

**Abstract**—We have calculated the effect that convection electric fields have on the velocity distribution of auroral ions at the altitudes where the plasma is weakly-ionized and where the various ion-neutral collision frequencies are much smaller than the ion cyclotron frequencies, i.e. between about 130 and 300 km. The appropriate Boltzmann equation has been solved by expanding the ion velocity distribution function in a generalized orthogonal polynomial series about a bi-Maxwellian weight factor. We have retained enough terms in the series expansion to enable us to obtain reliable quantitative results for electric field strengths as large as 90 mV m$^{-1}$. Although we have considered a range of ion–neutral scattering mechanisms, our main emphasis has been devoted to the long-range polarization interaction. In general, we have found that to lowest order the ion velocity distribution is better represented by a two-temperature or bi-Maxwellian distribution than by a one-temperature Maxwellian, with there being different ion temperatures parallel and perpendicular to the geomagnetic field. However, the departures from this zeroth-order bi-Maxwellian distribution become significant when the ion drift velocity approaches (or exceeds) the neutral thermal speed.

## 1. INTRODUCTION

Interest in the extent to which auroral ion velocity distributions depart from a Maxwellian was generated when Cole (1971) calculated ion velocity distributions for a collisionless plasma in crossed electric and magnetic fields. Since collisions were neglected, the resulting ion velocity distribution was time dependent and oscillated with the ion gyrofrequency. In order to apply his calculations to the auroral ionosphere, Cole extrapolated his results to a steady state, and then predicted large departures from the Maxwellian form for perpendicular electric fields as small as 10 mV m$^{-1}$. However, it was later shown that his results were valid only for small electric field strengths and for a small region of velocity space around the peak of the distribution (St-Maurice and Schunk, 1973).

Schunk and Walker (1972) calculated auroral ion velocity distributions for the lower ionosphere including the effects of ion–neutral collisions. In this study, the ion–neutral collision process was described by the Boltzmann collision integral, and a solution to Boltzmann's equation was obtained by expanding the ion distribution function in an orthogonal polynomial series about a Maxwellian weighting function. Since a Maxwellian weighting function was used and only a few terms in the series expansion were considered, Schunk and Walker were restricted to small departures of the distribution function from a Maxwellian and, hence, small electric field strengths or large ion-neutral collision frequencies. Nevertheless, these authors were able to determine the conditions under which departures become significant and the nature of these departures, and it was found that non-Maxwellian effects become appreciable for electric field strengths greater than about 10 mV m$^{-1}$.

In order to study situations where the ion distribution function departs significantly from a Maxwellian, St-Maurice and Schunk (1973, 1974) replaced the Boltzmann collision integral with a simple relaxation collision model and thereby were able to obtain an exact solution to Boltzmann's equation. In this way, it was found that the ion velocity distribution becomes highly non-Maxwellian when the ion drift velocity is comparable to or greater than the neutral thermal speed. For large electric fields and small collision to cyclotron frequency ratios, the ion distribution takes

* Present address: Physics Department, Utah State University, Logan, UT 84322, U.S.A.

the shape of a torus in velocity space, while for large electric fields and comparable collision and cyclotron frequencies the ion distribution is bean-shaped.

Although the simple relaxation collision model may be realistic for resonant charge exchange collisions, the Boltzmann collision integral is more appropriate for non-resonant interactions between ions and neutrals, such as between $NO^+$ and O. This latter collision combination is particularly important, since recent theoretical calculations by Schunk *et al.* (1975, 1976) indicate that large electric fields result in enhanced $NO^+$ densities due to the energy dependence of the $O^+ + N_2 \rightarrow NO^+ + N$ reaction rate. For the right conditions, $NO^+$ can even become the dominant ion throughout the *E*- and *F*-regions.

Recently, we have presented a method of solution of Boltzmann's equation that is valid for arbitrarily large departures of the velocity distribution function from a Maxwellian and arbitrary collision models (St-Maurice and Schunk, 1976). The method of solution consists of expanding the ion velocity distribution function in a generalized orthogonal polynomial series about an arbitrary weight factor. The exact form of the weight factor depends on the specific details of the problem. For a Maxwellian weight factor, the generalized orthogonal polynomial series is equivalent to Grad's expansion (Grad, 1958).

In the present investigation, we apply the generalized orthogonal polynomial method to the calculation of auroral ion velocity distributions, with particular emphasis given to non-resonant or polarization ion–neutral interactions. With this method, we are able to present more accurate expressions for $NO^+$ and $O^+$ velocity distribution functions than previously available. Although the method can be applied for arbitrary electric field strengths, large electric fields result in highly anisotropic velocity distribution functions, which are unstable (Ott and Farley, 1975). Consequently, we only consider electric field strengths for which the resulting ion velocity distributions are likely to be stable. The maximum electric field for which our results are valid depends on the properties of the ion–neutral scattering mechanism and, therefore, is different for different ion–neutral combinations.

Evidence for the presence in the auroral regions of a non-Maxwellian ion velocity distribution has now been presented by Swift (1975) and St-Maurice *et al.* (1976). The detection of non-Maxwellian distributions qualitatively similar to those described by St-Maurice and Schunk (1973, 1974) makes more pressing the need for accurate theoretical calculations in order to determine the extent to which various high latitude processes are affected. Theoretical expressions are required, for example, for the determination of ion-molecule reaction rates and for the excitation rates of various auroral processes (cf. Cole, 1971). The non-Maxwellian character of the velocity distribution along the magnetic field line is also important for the interpretation of ground-based measurements, such as the spectrum of radar waves incoherently scattered from the ionosphere. Furthermore, since the instability predicted by Ott and Farley (1975) depends very sensitively on the shape of the ion velocity distribution, more accurate theoretical expressions are needed to determine whether or not ion-neutral collisions can, in fact, produce the required anisotropy in the ion velocity distribution at a realistic value of the electric field.

In Section 2 we obtain a generalized orthogonal polynomial solution of Boltzmann's equation. In Section 3 we discuss ion-neutral scattering cross sections. Section 4 is devoted to a discussion of ion velocity distribution contours for various collision models with constant collision frequencies. Finally, in Section 5, we present a summary and conclusions.

## 2. THEORETICAL FORMULATION

To model auroral conditions at *E*- and *F*1-region altitudes, we consider a weakly-ionized plasma that has been subjected to crossed electric and magnetic fields. Since the plasma is weakly-ionized, we can solve Boltzmann's equation for each ion species independently of the other charged species. For a steady state, spatially homogeneous plasma, the appropriate Boltzmann equation is

$$[\boldsymbol{\Gamma}_i + \mathbf{c}_i \times \boldsymbol{\Omega}_i + \langle \mathbf{v}_i \rangle \times \boldsymbol{\Omega}_i] \cdot \nabla_{c_i} f_i = \frac{\delta f_i}{\delta t}, \tag{1}$$

where

$$\boldsymbol{\Gamma}_i = \frac{e_i \mathbf{E}_\perp}{m_i} \tag{2}$$

$$\boldsymbol{\Omega}_i = \frac{e_i \mathbf{B}}{m_i c} \tag{3}$$

$$\mathbf{c}_i = \mathbf{v}_i - \langle \mathbf{v}_i \rangle \tag{4}$$

and where $f_i(\mathbf{c}_i)$ is the distribution function of ion species $i$, $\mathbf{v}_i$ is the velocity, $\mathbf{c}_i$ is the random velocity, $\langle \mathbf{v}_i \rangle$ is the average drift velocity, $\nabla_{c_i}$ is the gradient operator in velocity space, $m_i$ is the ion mass, $e_i$ is the ion charge, $\mathbf{E}_\perp$ is the perpendicular electric field, $\mathbf{B}$ is the geomagnetic field, $c$ is the speed of light, and $\delta f_i/\delta t$ accounts for the rate of

change of $f_i$ due to ion-neutral collisions. In equation (4), the bracket symbol denotes the average

$$\langle \mathbf{A} \rangle = \frac{1}{n_i} \int d\mathbf{c}_i f_i \mathbf{A}. \tag{5}$$

For binary elastic collisions between ions and neutrals, the appropriate collision term is the Boltzmann collision integral

$$\frac{\delta f_i}{\delta t} = \int d\mathbf{v}_n \, d\Omega g_{in} \sigma_{in}(g_{in}, \theta)[\bar{f}_i \bar{f}_n - f_i f_n], \tag{6}$$

where the subscript $n$ denotes the neutral species, $d\mathbf{v}_n$ is the volume element in velocity space, $d\Omega$ is an element of solid angle in the center-of-mass reference frame, $\theta$ is the center-of-mass scattering angle, $g_{in}$ is the relative velocity of the colliding particles $i$ and $n$, $\sigma_{in}(g_{in}, \theta)$ is the differential scattering cross section, and the bars denote quantities evaluated after a collision. In its present form, Boltzmann's collision integral can be applied to arbitrary elastic scattering mechanisms. In our study, however, our main concern is for ion-neutral collision processes dominated by the long-range polarization interaction (Dalgarno *et al.*, 1958). With this so-called Maxwell molecule interaction, the ion-neutral collision frequency, $\nu_{in}$, is independent of velocity. In addition, we consider only one neutral species, but the generalization to several neutral species is straightforward.

In the present investigation, we also confine our attention to the $\nu_{in}/\Omega_i \to 0$ limit. As $\nu_{in}/\Omega_i \to 0$, the ion distribution in velocity space becomes symmetric about an axis that is parallel to the magnetic field direction and that passes through the $\mathbf{E}_\perp \times \mathbf{B}$ drift point (Chapman and Cowling, 1970). The consideration of this limit restricts the application of our results to altitudes above about 150 km.

Because of the cylindrical symmetry, it is convenient to introduce a cylindrical coordinate system with its axis along the magnetic field and its origin at the $\mathbf{E}_\perp \times \mathbf{B}$ drift point. This coordinate system is shown in Fig. 1. In this figure, the ion velocity components in the $\mathbf{E}_\perp \times \mathbf{B}$, $\mathbf{E}_\perp$, and $\mathbf{B}$ directions are denoted by $v_x$, $v_y$ and $v_z$, respectively. The quantity $D = E_\perp c/B$ is the magnitude of the ion drift velocity in the $\mathbf{E}_\perp \times \mathbf{B}$ direction, and $c_\perp$ and $\alpha$ are the magnitude and phase, respectively, of the component of the ion velocity perpendicular to $\mathbf{B}$ but measured relative to the $\mathbf{E}_\perp \times \mathbf{B}$ drift velocity.

In cylindrical coordinates and for $\nu_{in}/\Omega_i \ll 1$, Boltzmann's equation (1) becomes

$$-\Omega_i \frac{\partial f_i}{\partial \alpha} = \frac{\delta f_i}{\delta t}. \tag{7}$$

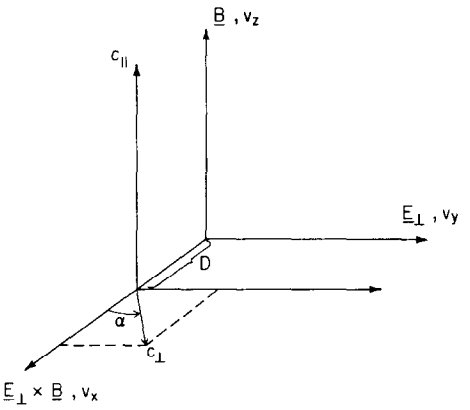


FIG. 1. ION VELOCITY–SPACE COORDINATE SYSTEM.

The quantities $(v_x, v_y, v_z)$ are the ion velocity components in the $\mathbf{E}_\perp \times \mathbf{B}$, $\mathbf{E}_\perp$ and $\mathbf{B}$ directions, respectively, $D$ is the magnitude of the $\mathbf{E}_\perp \times \mathbf{B}$ drift velocity, and $(c_\parallel, c_\perp, \alpha)$ are the ion velocity components for a cylindrical coordinate system with its origin at the $\mathbf{E}_\perp \times \mathbf{B}$ drift point.

The collision term on the right-hand side of equation (7) is of order $\nu_{in}/\Omega_i$ in comparison with the term on the left-hand side. This fact suggests that we seek a solution to equation (7) of the form

$$f_i = f_i^{(0)} + \frac{\nu_{in}}{\Omega_i} f_i^{(1)} + \ldots. \tag{8}$$

Substituting this series into equation (7) and equating like powers of $\nu_{in}/\Omega_i$, we obtain, to lowest order,

$$\frac{\partial f_i^{(0)}}{\partial \alpha} = 0 \tag{9}$$

which indicates that to lowest order the ion distribution function is symmetric about an axis that passes through the $\mathbf{E}_\perp \times \mathbf{B}$ drift point and is parallel to $\mathbf{B}$.

To next order, we obtain

$$-\Omega_i \frac{\partial f_i^{(1)}}{\partial \alpha} = \frac{\delta f_i^{(0)}}{\delta t}. \tag{10}$$

Since $f_i$ must be a single valued function of $\alpha$, the integral of the left-hand side of equation (10) over $\alpha$ from 0 to $2\pi$ is zero. Therefore, equation (10) can also be written as

$$\int_0^{2\pi} d\alpha \frac{\delta f_i^{(0)}}{\delta t} = 0, \tag{11}$$

where the collision term is given by equation (6).

Our original Boltzmann equation (1) has now been replaced by equations (9) and (11). To solve

these equations, we use the generalized orthogonal polynomial technique described by St-Maurice and Schunk (1976). With this technique, the ion velocity distribution function is expanded in a generalized orthogonal polynomial series about a given weight factor. In general, the form of the weight factor depends on the specific details of the problem. For the present case, it is easy to establish that the electric field causes a temperature anisotropy and, therefore, it is reasonable to assume that to lowest order the ion velocity distribution is bi-Maxwellian. Consequently, the weight factor of our generalized orthogonal polynomial series is taken as

$$w = \exp\left[-(c_\parallel'^2 + c_\perp^{*2})\right] \tag{12}$$

where

$$c_\parallel' = c_\parallel/(2kT_\parallel/m_i)^{1/2} \tag{13}$$

$$c_\perp^* = c_\perp/(2kT_\perp/m_i)^{1/2} \tag{14}$$

and where $k$ is Boltzmann's constant and $T_\parallel$ and $T_\perp$ are, as yet, unspecified temperatures parallel and perpendicular to the magnetic field. In equations (12) to (14) and all subsequent equations, the subscript $i$ is dropped from the ion random velocity components for simplicity.

Since the weight factor is separable with respect to the ion velocity components $c_\parallel'$ and $c_\perp^*$, the series expansion for the ion distribution function will contain a product of polynomials. For the velocity component along the magnetic field, the appropriate orthogonal polynomials are the Hermite polynomials, $H_m(c_\parallel')$, while for the ion velocity component perpendicular to the magnetic field the appropriate orthogonal polynomials are the associated Laguerre polynomials of degree zero, $L_n^0(c_\perp^{*2})$, (cf. St-Maurice and Schunk, 1976). The Hermite and associated Laguerre polynomials are defined in Appendix A.

Using the bi-Maxwellian weight factor (12) and the appropriate polynomials, the orthogonal polynomial series expansion for the ion distribution function becomes

$$f_i(c_\parallel', c_\perp^*) = \exp\left[-(c_\parallel'^2 + c_\perp^{*2})\right] \times \sum_{m=0}^{\infty}\sum_{n=0}^{\infty} a_{mn} H_m(c_\parallel') L_n^0(c_\perp^{*2}), \tag{15}$$

where $a_{mn}$ is an expansion coefficient. The expansion coefficients can be expressed in terms of moments of the distribution function by multiplying equation (15) with the appropriate combination of Hermite and associated Laguerre polynomials and by integrating over velocity space,

$$a_{mn} = \frac{2^{(1-m)}}{m!\sqrt{\pi}[\Gamma(n+1)]^2} \int_{-\infty}^{\infty} dc_\parallel' H_m(c_\parallel') \times \int_0^{\infty} dc_\perp^* c_\perp^* L_n^0(c_\perp^{*2}) f_i(c_\parallel', c_\perp^*), \tag{16}$$

where use has been made of the orthogonality relations of the Hermite (equation A7) and associated Laguerre (equation A14) polynomials and where $\Gamma(X)$ is the gamma function.

Explicit expressions for the expansion coefficients in terms of the velocity moments can be obtained from equation (16) by using the Hermite and associated Laguerre polynomials given in Appendix A. Since the ion distribution function is symmetric about the velocity plane $c_\parallel' = 0$, all odd velocity moments of $c_\parallel$ are zero, and, consequently, many of the expansion coefficients are zero. The first few non-zero expansion coefficients are given by

$$a_{00} = \frac{n_i}{\pi^{3/2}} \tag{17a}$$

$$a_{01} = \frac{n_i}{\pi^{3/2}}[1 - \langle c_\perp^{*2}\rangle] \tag{17b}$$

$$a_{02} = \frac{n_i}{4\pi^{3/2}}[2 - 4\langle c_\perp^{*2}\rangle + \langle c_\perp^{*4}\rangle] \tag{17c}$$

$$a_{20} = \frac{n_i}{8\pi^{3/2}}[4\langle c_\parallel'^2\rangle - 2] \tag{17d}$$

$$a_{21} = \frac{n_i}{8\pi^{3/2}}[4\langle c_\parallel'^2\rangle + 2\langle c_\perp^{*2}\rangle - 4\langle c_\parallel'^2 c_\perp^{*2}\rangle - 2] \tag{17e}$$

$$a_{40} = \frac{n_i}{384\pi^{3/2}}[12 - 48\langle c_\parallel'^2\rangle + 16\langle c_\parallel'^4\rangle], \tag{17f}$$

where the bracket symbol is defined by equation (5), provided $f_i \to f_i(c_\parallel', c_\perp^*)$ and $d\mathbf{c}_i \to c_\perp^*\, dc_\perp^*\, dc_\parallel'\, d\alpha$.

Up to this point, we have not defined $T_\parallel$ and $T_\perp$. The definition of these temperatures is arbitrary and, in general, it is useful to define these quantities in such a way as to obtain a more rapidly converging series. For our purpose, it is useful to define $T_\parallel$ and $T_\perp$ as the ion temperatures $T_{i\parallel}$ and $T_{i\perp}$ obtained by taking the parallel and perpendicular energy moments of Boltzmann's equation. With this choice,

$$\langle c_\perp^{*2}\rangle = 1 \tag{18}$$

$$\langle c_\parallel'^2\rangle = \tfrac{1}{2} \tag{19}$$

and, as a consequence, the expansion coefficients

(17) become

$$a_{00} = \frac{n_i}{\pi^{3/2}} \tag{20a}$$

$$a_{02} = \frac{n_i}{4\pi^{3/2}}[\langle c_\perp{}^{*4}\rangle - 2] \tag{20b}$$

$$a_{21} = \frac{n_i}{4\pi^{3/2}}[1 - 2\langle c_\parallel{}'^2 c_\perp{}^{*2}\rangle] \tag{20c}$$

$$a_{40} = \frac{n_i}{96\pi^{3/2}}[4\langle c_\parallel{}'^4\rangle - 3] \tag{20d}$$

$$a_{01} = a_{20} = 0. \tag{20e}$$

The velocity moments appearing in the expressions for the expansion coefficients can be expressed in terms of the electric field by taking moments of Boltzmann's equation (equations 9 and 11, with the collision term given by equation 6). For the present case, the evaluation of the velocity moments is complex from the algebraic point of view because it is necessary to consider fourth-order tensors. We therefore outline the procedure for calculating the velocity moments in Appendix B.

When just the expansion coefficients given by equation (17 or 20) are considered, the orthogonal polynomial series expansion of the ion velocity distribution function becomes

$$f_i(c_\parallel', c_\perp{}^*) = a_{00}\exp[-(c_\parallel{}'^2 + c_\perp{}^{*2})]\left\{1 + \frac{a_{01}}{a_{00}}(1 - c_\perp{}^{*2}) + \frac{a_{02}}{a_{00}}(2 - 4c_\perp{}^{*2} + c_\perp{}^{*4}) + \frac{a_{20}}{a_{00}}(4c_\parallel{}'^2 - 2) + \frac{a_{21}}{a_{00}}(4c_\parallel{}'^2 - 2)(1 - c_\perp{}^{*2}) + \frac{a_{40}}{a_{00}}(12 - 48c_\parallel{}'^2 + 16c_\parallel{}'^4)\right\}, \tag{21}$$

where we have used the expressions for the Hermite and associated Laguerre polynomials given in Appendix A and where the non-dimensional ion velocity components $(c_\parallel', c_\perp{}^*)$ are defined by equations (13) and (14). The series expansion (21) is the expression for the ion velocity distribution used in the present investigation. In this series, all velocity moments up to fourth-order are included.

### 3. ION–NEUTRAL SCATTERING CROSS SECTIONS

In order to calculate ion velocity distributions for arbitrary collision models, it is necessary to know the relevant ion–neutral scattering cross sections $Q_{in}^{(l)}$ (see Appendix B). For auroral ionospheric applications, the important E- and F1-region ions are $NO^+$, $O_2{}^+$, $N_2{}^+$ and $O^+$, while at the altitudes of interest in the present study (altitudes for which $\nu_{in}/\Omega_i \ll 1$) the dominant neutral species are atomic oxygen and molecular nitrogen. In the following subsections, we briefly discuss the calculation of the appropriate ion-neutral scattering cross sections. For completeness, we also consider certain limiting cases in order to cover a range of scattering mechanisms.

*Polarization attraction*

For collisions of $NO^+$, $O_2{}^+$ and $N_2{}^+$ with neutral atomic oxygen, the scattering process probably consists of a long-range polarization attraction and a short-range repulsion (Mason, 1970). In the classical limit, a pure polarization attraction yields scattering cross sections that vary as $Q_{in}^{(l)} \sim 1/g_{in}$ for all values of $l$, where $g_{in}$ is the non-neutral relative speed. With this so-called Maxwell molecule interaction, the ion-neutral collision frequency is independent of velocity and, as a consequence, the calculation of ion velocity distributions is significantly simplified. It is therefore useful to study the extent to which the ion–neutral interaction can be considered to be a Maxwell molecule interaction.

Non-Maxwell molecule behaviour can arise from two processes. First, quantum effects introduce modifications. Quantum effects are important for grazing incidence collisions, but the factor $(1 - \cos^l\theta)$ in the expression for the scattering cross section (B18) makes the quantum contribution unimportant near $\theta = 0$ (McDaniel and Mason, 1973; p. 128). Quantum effects also introduce resonances, which appear as short scale oscillations in $Q_{in}^{(l)}$. These are particularly important when the relative ion–neutral energy is small compared to the depth of the potential of interaction, $\varepsilon$. In general, however, for $T_i \gtrsim 300$ K the oscillations average out to the classical limit when $Q_{in}^{(l)}$ is integrated over an energy range (McDaniel and Mason, 1973; p. 222).

Non-Maxwell molecule behaviour can also arise from the presence of short-range repulsive forces in the ion–neutral interaction. The effect of short-range repulsion is shown in Fig. 2, where we present $Q_{in}^{(1)}$ as a function of the relative kinetic energy, $\frac{1}{2}\mu_{in}g_{in}{}^2$, for various models of the polarization-short range interaction. In the expression for the relative kinetic energy, $\mu_{in} = m_i m_n/(m_i + m_n)$ is the non-neutral reduced mass. In Fig. 2, the relative kinetic energy is normalized with respect to $\varepsilon$ and $Q_{in}^{(1)}$ is normalized with respect to $\pi r_m{}^2$, where $r_m$ is the interaction distance for which the potential of interaction is a minimum, i.e. $-\varepsilon$.

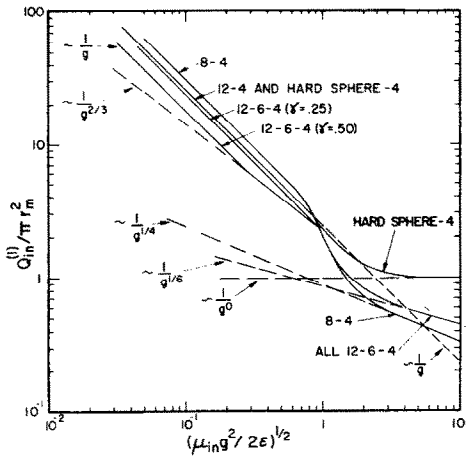


FIG. 2. ENERGY DEPENDENCE OF THE MOMENTUM TRANSFER CROSS SECTION, $Q_{in}^{(1)}$, FOR VARIOUS MODELS OF THE POLARIZATION–HARD CORE INTERACTION.

In this figure, $Q_{in}^{(1)}$ is non-dimensionalized with respect to $\pi r_m^2$, where $r_m$ is the value of $r$ for which the potential energy is a minimum. For the hard sphere, we selected a radius equal to $r_m$ for a 12–4 interaction. The parameter $\mu_{in} g_{in}^2/2\varepsilon$ is the non-dimensional energy, where $\varepsilon$ is the minimum value of the interaction potential.

For the models shown in Fig. 2, the repulsive potential is assumed to be proportional to $1/r^n$, where $n = 8$, 12, or $\infty$ (hard sphere). The attractive potential in most cases is just that due to polarization attraction, which is proportional to $1/r^4$. However, in the 12–6–4 models, Mason and Schamp (1958) added an attractive component proportional to $1/r^6$ in order to allow for dispersion forces. In these models, the constant $\gamma$ reflects relative strength of the $1/r^6$ potential when the relative kinetic energy is asymptotically small. The hard-sphere-4 model was used by Langevin (1905), while the 8–4 model was used by Hassé and Cook (1931).

It is apparent from Fig. 2 that all the models contain a transition region in which the interaction changes from purely attractive to purely repulsive. The "softer" the repulsion, the larger the transition region and the greater the departure of $Q_{in}^{(1)}$ from a

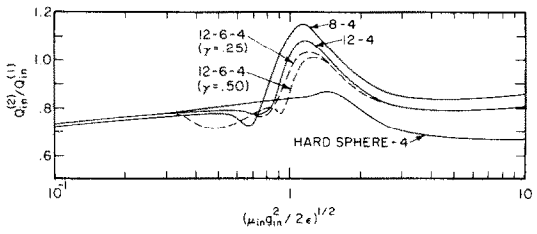


FIG. 3. ENERGY DEPENDENCE OF $Q_{in}^{(2)}/Q_{in}^{(1)}$ FOR VARIOUS POLARIZATION–HARD CORE MODELS.

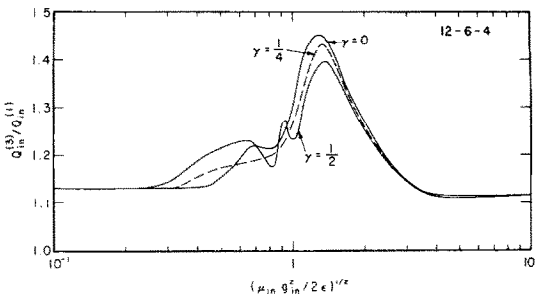


FIG. 4. ENERGY DEPENDENCE OF $Q_{in}^{(3)}/Q_{in}^{(1)}$ FOR VARIOUS POLARIZATION–HARD CORE MODELS.

$1/g_{in}$ dependence in the transition region. The reason for this behavior has been discussed in detail by Wannier (1970) and will not be repeated here. The important point to note is that the departure of $Q_{in}^{(1)}$ from a $1/g_{in}$ dependence is not too significant (less than 40% for a 12–4 potential) for relative kinetic energies less than about $10\varepsilon$. As discussed below, this energy range covers typical relative kinetic energies found in the ambient high-latitude plasma, and, consequently, for most auroral applications it is sufficient to assume that $Q_{in}^{(1)}$ varies as $1/g_{in}$, with the constant of proportionality given by the mean of the actual velocity dependent quantity $Q_{in}^{(1)} g_{in}$. The calculation of the mean is discussed below.

The behaviour of the scattering cross sections $Q_{in}^{(2)}$, $Q_{in}^{(3)}$ and $Q_{in}^{(4)}$ as a function of relative kinetic energy is similar to that shown in Fig. 2 for $Q_{in}^{(1)}$. However, the departure of these cross sections from a $1/g_{in}$ dependence in the transition region is smaller than that of $Q_{in}^{(1)}$. Also, the effect of the hard core is not felt in exactly the same way. For these reasons, the ratio $Q_{in}^{(l)}/Q_{in}^{(1)}$ $(l>1)$ exhibits structure, with a peak value occurring in the transition region. This behaviour is shown in Figs. 3–5 for

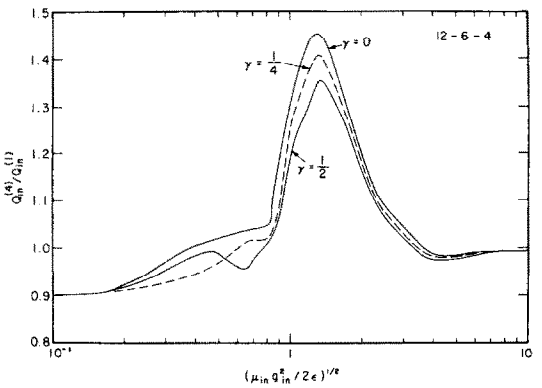


FIG. 5. ENERGY DEPENDENCE OF $Q_{in}^{(4)}/Q_{in}^{(1)}$ FOR VARIOUS POLARIZATION–HARD CORE MODELS.

the various interaction models that have been considered to date. As with $Q_{in}^{(1)}$, the velocity dependent quantities $Q_{in}^{(l)}g_{in}$ $(l>1)$ can be replaced by their mean values.

In order to determine mean values for $Q_{in}^{(l)}g_{in}$, we must know both the value of the potential minimum, $-\varepsilon$, and the mean relative energy, $\bar{E}_{in}$, for various temperature regimes. For non-resonant collisions between $O^+$, $NO^+$, $O_2^+$ or $N_2^+$ and neutral atomic oxygen and molecular nitrogen $\varepsilon$ apparently falls in the range 0.05–0.1 eV (Mason, 1970). To evaluate $\bar{E}_{in}$ we use the formula given by McFarland *et al.* (1973), which relates the mean relative energy to the ion and neutral temperatures and the $\mathbf{E}_\perp \times \mathbf{B}$ drift velocity. Since the ion temperature, in turn, depends on the neutral temperature and the $\mathbf{E}_\perp \times \mathbf{B}$ drift velocity, it is easy to show that $\bar{E}_{in} = 3kT_i/2$.

For a given ion-neutral collision pair, the mean values of $Q_{in}^{(l)}g_{in}$ are calculated by first selecting a value for $\varepsilon$ and then choosing an appropriate mean relative energy (or ion temperature) range. Typically, the curves of $Q_{in}^{(l)}$ vs energy can be divided into three distinct energy regimes and, consequently, there are three sets of $Q_{in}^{(l)}/Q_{in}^{(1)}$ ratios for each value of $\varepsilon$. Since $\varepsilon$ itself is not precisely known for a given ion-neutral pair, variations of $\varepsilon$ within the allowable range of 0.05–0.1 eV should also be considered. In Table 1 we show three sets of $Q_{in}^{(l)}/Q_{in}^{(1)}$ ratios for our so-called "polarization" interaction (12–4 interaction potential). The sets shown tend to cover the range of possible values and, therefore, are indicative of the uncertainty associated with the determination of the scattering cross section ratios for a polarization interaction. Fortunately, our results are not very sensitive to changes in the $Q_{in}^{(l)}/Q_{in}^{(1)}$ ratios within the limits shown in Table 1. In subsequent velocity distribution calculations, we adopt the $Q_{in}^{(l)}/Q_{in}^{(1)}$ values labeled "polarization (model B)" for all non-resonant ion–neutral interactions.

TABLE 1. SCATTERING CROSS SECTION RATIOS FOR VARIOUS COLLISION MODELS

| Model | $Q_{in}^{(2)}/Q_{in}^{(1)}$ | $Q_{in}^{(3)}/Q_{in}^{(1)}$ | $Q_{in}^{(4)}/Q_{in}^{(1)}$ |
|---|---|---|---|
| Relaxation | 0 | 1 | 0 |
| Resonant charge exchange (Model A) | 0.45 | 1 | 0.55 |
| Resonant charge exchange (Model B) | 0.30 | 1 | 0.40 |
| Polarization (Model A) | 0.80 | 1.2 | 1.1 |
| Polarization (Model B) | 0.95 | 1.3 | 1.3 |
| Polarization (Model C) | 1.05 | 1.45 | 1.45 |
| Forward scattering | 2 | 3 | 4 |

*Resonant charge exchange*

For collisions between an ion and its parent neutral, both resonant charge exchange and elastic scattering are possible. For resonant charge exchange, Dalgarno (1958) has shown that to leading order the momentum transfer cross section, $Q_{in}^{(1)}$, is twice the charge exchange cross section, $Q_E$, defined by

$$Q_E = 2\pi \int_0^\pi \sigma_E(g_{in}, \theta) \sin\theta \, d\theta, \tag{22}$$

where $\sigma_E(g_{in}, \theta)$ is the differential cross section for charge exchange. In the classical sense, this relation between $Q_{in}^{(1)}$ and $Q_E$ implies that

$$\sigma_E(g_{in}, \theta) = C_E(g_{in})\, \delta(\theta - \pi), \tag{23}$$

where $C_E(g_{in})$ is a slowly varying logarithmic function of $g_{in}$ (cf. Banks, 1966; Banks and Kocharts, 1973) and $\delta$ is the delta function. In our ion velocity distribution calculations, the logarithmic dependence of $C_E$ on $g_{in}$ is replaced with a polarization dependence. This change, which significantly simplifies the algebra, does not introduce significant errors if $\nu_{in}/\Omega_i$ is small (cf. St-Maurice, 1975), as is assumed here.

Although the charge exchange cross section is much larger than the elastic scattering cross section for typical ionospheric ion and neutral temperatures, the $\theta$-dependence of $\sigma_E$ indicates that the charge exchange contribution to $Q_{in}^{(l)}$ vanishes when $l$ is even (see equation B18). Consequently, for even values of $l$, $Q_{in}^{(l)}$ is calculated for an elastic scattering mechanism, while for odd $l$ it is calculated for a charge exchange mechanism (Mason *et al.*, 1959).

The calculation of $Q_{in}^{(l)}$ for odd $l$ follows directly from equations (23) and (B18) and the expression for $\sigma_E$ given by Banks (1966). For even $l$, on the other hand, $Q_{in}^{(l)}$ is calculated in the manner described in the previous subsection on polarization interactions. For $O^+$–O interactions, valence attraction is probably the dominant elastic scattering mechanism and, therefore, the potential minimum, $\varepsilon$, probably is of the order of 2–3 volts (cf. Mason, 1970). In this case, $Q_{in}^{(l)}$ for even $l$ can be obtained from Figs. 2, 3 and 5 using the limit $(\frac{1}{2})\mu_{in}g_{in}^2 \ll \varepsilon$.

As with our previous polarization models, more than one set of $Q_{in}^{(l)}/Q_{in}^{(1)}$ ratios is possible for $O^+$–O interactions. In Table 1 we present two sets; resonant charge exchange models A and B. Model A is

for $T_i \leqslant 2500$ K, while model B is for $T_i \geqslant 3000$ K. Since the $T_i$ range of model A is more appropriate for the electric field strengths considered in this investigation, we use resonant charge exchange model A for all ion velocity distribution calculations dealing with $O^+$–O interactions.

*Relaxation model*

In order to compare our results with previous work, it is useful to evaluate the scattering cross sections for a relaxation collision model (St-Maurice and Schunk, 1973, 1974). It is easy to show that the relaxation collision model can be derived directly from the Boltzmann collision integral by assuming equal ion and neutral masses and adopting a differential scattering cross section of the form

$$\sigma_{RM} = C_{RM}\,\delta(\theta-\pi)/g_{in}, \tag{24}$$

where $C_{RM}$ is a constant. It follows directly from equations (24) and (B18) that

$$Q^{(3)}_{RM} = Q^{(1)}_{RM} \tag{25}$$

and

$$Q^{(4)}_{RM} = Q^{(2)}_{RM} = 0. \tag{26}$$

Scattering cross section ratios for the relaxation model are summarized in Table 1.

The relaxation model is a back-scattering collision model with a constant collision frequency. It approximates a resonant charge exchange collision process in the limit of very high ion temperatures despite the fact that the resonant charge exchange collision frequency is velocity dependent.

*Forward scattering model*

For completeness we also consider a forward-scattering collision model with a constant collision frequency. The differential scattering cross section for such a model takes the form

$$\sigma_{FS} = C_{FS}\,\delta(\theta)/g_{in}, \tag{27}$$

where $C_{FS}$ is a constant. Substituting equation (27) into (B18), we obtain

$$Q^{(l)}_{in}/Q^{(1)}_{in} = l. \tag{28}$$

The scattering cross section ratios given by equation (28) correspond to the classical limit of forward scattering. If forward scattering was a dominant feature of an actual collision process, quantum effects would have to be considered. Consequently, our forward scattering model is not a physically realistic collision model. Nevertheless, this model is useful since its scattering property is opposite to that of the relaxation model and, therefore, with the two models we are able to bracket the complete range of classical scattering behavior.

## 4. ION VELOCITY DISTRIBUTIONS

### 4.1. *Comparison with a Maxwellian*

Our new expression for the ion velocity distribution function (equation 21) corresponds to an orthogonal polynomial series expansion about a bi-Maxwellian weighting function. Since only a limited number of terms in the infinite series are retained, it is important to establish that the resulting truncated series can properly describe distributions that differ significantly from a Maxwellian. For this reason, it is useful to first consider the relaxation collision model (cf. St-Maurice and Schunk, 1973, 1974).

The relaxation model results will first be compared to a Maxwellian distribution which has the same density, drift velocity, and energy moments as the actual distribution. This Maxwellian has the form

$$f_M(\mathbf{c}_i) = n_i\left(\frac{m_i}{2\pi kT_i}\right)^{3/2}\exp\left[-\frac{m_i c_i^2}{2kT_i}\right], \tag{29}$$

where $T_i$ is the ion temperature,

$$\tfrac{3}{2}kT_i = \tfrac{1}{2}m_i\langle c_i^2\rangle. \tag{30}$$

Since the energy moments of $f_i$ and $f_M$ are the same, we have

$$T_i = (T_{i\parallel} + 2T_{i\perp})/3. \tag{31}$$

The results obtained from our series expansion (21) for the relaxation collision model are shown in Fig. 6, where we present contours of $f_i/f_M$ in the principal $c_x$–$c_\parallel$ velocity plane. In this figure, $D' = D/v_{T_n}$ is the non-dimensional ion drift speed, $D = E_\perp c/B$ is the magnitude of the ion $\mathbf{E}_\perp \times \mathbf{B}$ drift velocity, $v_{T_n} = (2kT_n/m_n)^{1/2}$ is the neutral thermal speed, and $v_{T_i} = (2kT_i/m_i)^{1/2}$ is the ion thermal speed. The quantity $D'$ can be related to a specific value of $E_\perp$ if $T_n$ is known; this relationship is shown in Table 2. Also shown in Table 2 are the associated ion temperatures. Since both $f_i$ and $f_M$ are symmetric about the $c_\parallel$-axis, 3-dimensional contours of $f_i/f_M$ can be obtained from Fig. 6 by rotating these contours about the $c_\parallel$-axis. In this way, it is easy to see that the ion velocity distribution tends to take the shape of a torus in velocity space as the electric field strength is increased. This behaviour is in agreement with our previous relaxation model results, which were obtained from an exact solution to Boltzmann's equation (cf. St-Maurice and Schunk, 1973, 1974). A more detailed

TABLE 2. VALUES OF $E_\perp$(mV m$^{-1}$) AND $T_i$(K) AS A FUNCTION OF $D/v_{T_n}$ FOR ION INTERACTIONS WITH NEUTRAL ATOMIC OXYGEN

| $T_n$ = | 800 | | 1000 | | 1200 | | 1500 | |
|---|---|---|---|---|---|---|---|---|
| $D/v_{T_n}$ | $E_\perp$ | $T_i$ | $E_\perp$ | $T_i$ | $E_\perp$ | $T_i$ | $E_\perp$ | $T_i$ |
| 0.5 | 22.7 | 933 | 25.4 | 1167 | 27.8 | 1400 | 31.1 | 1750 |
| 1.0 | 45.4 | 1333 | 50.8 | 1667 | 55.6 | 2000 | 62.2 | 2500 |
| 1.5 | 68.1 | 2000 | 76.2 | 2500 | 83.4 | 3000 | 93.3 | 3750 |
| 2.0 | 90.8 | 2933 | 101.6 | 3667 | 111.3 | 4400 | 124.4 | 5500 |

quantitative comparison indicates that our series expansion of $f_i$ (equation 21) provides a good approximation to the actual velocity distribution function over a fairly large region of velocity space.

The precise area of velocity space in which our series converges depends on both the magnitude of the electric field and the ion-neutral collision model. For a given collision model, an increase in the electric field strength results in a greater departure of $f_i$ from our assumed zeroth-order bi-Maxwellian and this, in turn, results in a smaller region of convergence. For a given $E_\perp$, on the other hand, we show below that, in general, the relaxation collision model produces the greatest departure of $f_i$ from the zeroth-order bi-Maxwellian and, hence, yields the smallest region of convergence. Consequently, the fact that we are able to check the convergence of our series for the relaxation collision model gives us added confidence in the results we obtain for other collision models.

### 4.2. *Zeroth-order bi-Maxwellian*

Since the ion velocity distribution is bi-Maxwellian to lowest order, it is instructive to study the properties of this distribution. This zeroth-order bi-Maxwellian can be obtained from our series expansion (21) by setting all expansion coefficients equal to zero except $a_{00}$. When expressed in terms of the random velocity, this distribution takes the familiar form

$$f_{BM}(c_{i\parallel}, c_{i\perp}) = n_i\left(\frac{m_i}{2\pi kT_{i\perp}}\right)\left(\frac{m_i}{2\pi kT_{i\parallel}}\right)^{1/2} \times \exp\left[-\frac{m_i c_{i\parallel}^2}{2kT_{i\parallel}} - \frac{m_i c_{i\perp}^2}{2kT_{i\perp}}\right], \quad (32)$$

where the complete expressions for $T_{i\parallel}$ and $T_{i\perp}$ are given by equations (B21) and (B22), respectively. For a given ion–neutral collision model and mass ratio, the expressions for $T_{i\parallel}$ and $T_{i\perp}$ take a particularly simple form

$$T_{i\parallel} = T_n[1 + \beta_\parallel D'^2] \quad (33)$$

$$T_{i\perp} = T_n[1 + \beta_\perp D'^2], \quad (34)$$

where $\beta_\parallel$ and $\beta_\perp$ are pure numbers depending upon ion-neutral collision model and mass ratio; values are given in Table 3.

In effect, the values of $\beta$ determine the extent to which $T_{i\parallel}$ and $T_{i\perp}$ differ. The greatest temperature difference occurs for the relaxation collision model, where $\beta_\parallel = 0$ and $\beta_\perp$ assumes its maximum value, i.e. $\beta_\perp = 1$. For the relaxation model, the effect of a perpendicular electric field is concentrated in the perpendicular velocity plane, and $T_{i\parallel} = T_n$ for all electric field strengths. For other collision models, however, a perpendicular electric field affects both $T_{i\parallel}$ and $T_{i\perp}$. Assuming $m_i/m_n = 1$, for example, Table 3 indicates that the difference between $\beta_\parallel$ and $\beta_\perp$ and, hence, $T_{i\parallel}$ and $T_{i\perp}$ decreases as one goes from the relaxation model to the resonant charge exchange model, to the polarization model.

The progression from model to model in this order is essentially from back scattering toward forward scattering. For the three models considered, $T_{i\parallel} < T_{i\perp}$. However, a continuation of the

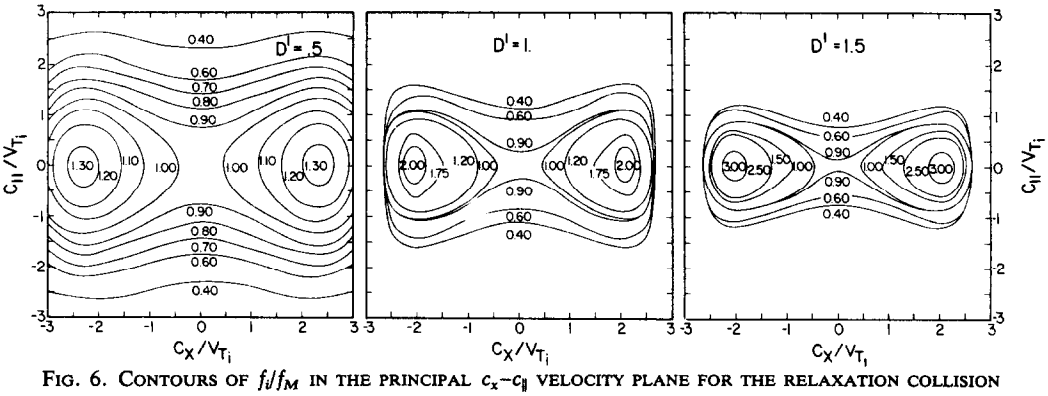


FIG. 6. CONTOURS OF $f_i/f_M$ IN THE PRINCIPAL $c_x$–$c_\parallel$ VELOCITY PLANE FOR THE RELAXATION COLLISION MODEL.

In this figure, $D' = D/v_{T_n}$, $D = E_\perp c/B$, $v_{T_n} = (2kT_n/m_n)^{1/2}$ and $v_{T_i} = (2kT_i/m_i)^{1/2}$.

TABLE 3. VALUES OF $\beta_\parallel$ AND $\beta_\perp$ FOR DIFFERENT COLLISION MODELS

| Model | $\beta_\parallel$ | $\beta_\perp$ |
|---|---|---|
| Relaxation | 0 | 1 |
| Resonant charge exchange | 0.3364 | 0.8318 |
| Polarization ($m_i/m_n \to 0$) | 2/3 | 2/3 |
| Polarization ($m_i/m_n = \frac{1}{2}$) | 0.5876 | 0.7062 |
| Polarization ($m_i/m_n = 1$) | 0.5547 | 0.7226 |
| Polarization ($m_i/m_n = 2$) | 0.5253 | 0.7373 |
| Polarization ($m_i/m_n \to \infty$) | 0.4750 | 0.7625 |
| Equal temperature | 2/3 | 2/3 |
| Forward scattering ($m_i/m_n = 1$) | 4/5 | 3/5 |

progression toward forward scattering leads to the so-called "equal temperature" model, for which $T_{i\parallel} = T_{i\perp}$. This equal temperature condition, which is obtained by setting $Q_{in}^{(2)}/Q_{in}^{(1)} = \frac{4}{3}$, holds for all electric field strengths and for arbitrary ion-neutral mass ratios. Finally, in the forward scattering limit, $T_{i\parallel} > T_{i\perp}$.

A more quantitative comparison of parallel and perpendicular ion temperatures is given in Tables 4 and 5. In Table 4, $T_{i\parallel}$ and $T_{i\perp}$ are presented as a function of $D'$ for different collision models and a single ion-neutral mass ratio ($m_i/m_n = 1$), while in Table 5 the effect of different ion-neutral mass ratios is shown for the polarization collision model. As discussed above, the relaxation model produces the greatest temperature difference, with $T_{i\perp} - T_{i\parallel} = 4000$ K for $D' = 2$. For resonant charge exchange, $(T_{i\perp} - T_{i\parallel})$ varies from 125 K for $D' = 0.5$ to approximately 2000 K for $D' = 2$, while for the polarization collision model $(T_{i\perp} - T_{i\parallel})$ varies from 42 to 670 K for the same values of $D'$. For the forward scattering model, $T_{i\parallel}$ is greater than $T_{i\perp}$, with the temperature difference varying from 50 to 800 K for the values of $D'$ shown.

With regard to the effect of the ion-neutral mass ratio, Table 5 indicates that relative to the results shown in Table 4 for $m_i/m_n = 1$ smaller mass ratios produce smaller $(T_{i\perp} - T_{i\parallel})$ differences, while the opposite is true for larger mass ratios. In the asymptotic limit of a light ion or massive neutral, the perpendicular–parallel temperature difference vanishes, while in the opposite limit of a heavy ion or light neutral perpendicular–parallel temperature differences of up to 1150 K are possible for the polarization collision model and $D' = 2$. However, for the ion–neutral mass ratios typical of $E$ and $F1$-region altitudes, $(T_{i\perp} - T_{i\parallel})$ varies from 474 K for $m_i/m_n = \frac{1}{2}$ to 848 K for $m_i/m_n = 2$, again for $D' = 2$.

The shape in velocity space of the zeroth-order bi-Maxwellian can be readily established by studying contours of $\log f_{BM}$ in the velocity planes parallel and perpendicular to **B**. In the principal velocity plane perpendicular to **B**, the contours form a family of concentric circles, since $f_{BM}$ exhibits cylindrical symmetry about the axis $c_{i\perp} = 0$. However, for any velocity plane that is parallel to **B** and passes through $c_{i\perp} = 0$, the contours form a family of ellipses, with the major and minor axes of the ellipses aligned parallel and perpendicular to **B**. For the physically realistic resonant charge exchange and polarization collision models, the major axes of the ellipses are perpendicular to **B**, since $T_{i\perp} > T_{i\parallel}$ for these collision models.

### 4.3. *Departures from a bi-Maxwellian*

The velocity–space contours of the actual ion velocity distribution will differ from the bi-Maxwellian contours to a degree which depends upon such parameters as the electric field strength and the ion–neutral scattering cross section and mass ratios. To study these departures, it is more convenient to plot contours of $f_i/f_{BM}$ rather than $f_i/f_M$, as was done earlier for the relaxation model. Furthermore, a plot of $f_i/f_{BM}$ is, in effect, a plot of the sum of the terms in our series expansion (21), and, therefore, the region of convergence of our series expansion can be simply determined by selecting that region of velocity space where the sum differs from the leading term (unity) by a specified amount. Typically, variations of $f_i/f_{BM}$ between 0.8 and 1.2 are reliable.

TABLE 4. PARALLEL AND PERPENDICULAR ION TEMPERATURES (K) AS A FUNCTION OF $D'$ FOR $m_i/m_n = 1$, $T_n = 1000$ K, AND FOR DIFFERENT COLLISION MODELS ($D' = D/v_{Tn}$; $D = E_\perp c/B$, $v_{Tn} = (2kT_n/m_n)^{1/2}$)

| | Relaxation | | Resonant charge exchange | | Polarization | | Equal temperature | | Forward scattering | |
|---|---|---|---|---|---|---|---|---|---|---|
| $D'$ | $T_{i\parallel}$ | $T_{i\perp}$ | $T_{i\parallel}$ | $T_{i\perp}$ | $T_{i\parallel}$ | $T_{i\perp}$ | $T_{i\parallel}$ | $T_{i\perp}$ | $T_{i\parallel}$ | $T_{i\perp}$ |
| 0.5 | 1000 | 1250 | 1084 | 1208 | 1139 | 1181 | 1167 | 1167 | 1200 | 1150 |
| 1.0 | 1000 | 2000 | 1336 | 1832 | 1555 | 1723 | 1667 | 1667 | 1800 | 1600 |
| 1.5 | 1000 | 3250 | 1757 | 2871 | 2248 | 2626 | 2500 | 2500 | 2800 | 2350 |
| 2.0 | 1000 | 5000 | 2346 | 4327 | 3219 | 3890 | 3667 | 3667 | 4200 | 3400 |

TABLE 5. PARALLEL AND PERPENDICULAR ION TEMPERATURES (K) AS A FUNCTION OF $D'$ AND $m_i/m_n$ FOR A POLARIZATION COLLISION MODEL WITH $T_n = 1000$ K ($D' = D/v_{T_n}$; $D = E_\perp c/B$, $v_{T_n} = (2kT_n/m_n)^{1/2}$)

| $m_i/m_n$ = | 0 | | $\frac{1}{2}$ | | 1 | | 2 | | $\infty$ | |
|---|---|---|---|---|---|---|---|---|---|---|
| $D'$ | $T_{i\parallel}$ | $T_{i\perp}$ | $T_{i\parallel}$ | $T_{i\perp}$ | $T_{i\parallel}$ | $T_{i\perp}$ | $T_{i\parallel}$ | $T_{i\perp}$ | $T_{i\parallel}$ | $T_{i\perp}$ |
| 0.5 | 1167 | 1167 | 1147 | 1177 | 1139 | 1181 | 1131 | 1184 | 1119 | 1191 |
| 1.0 | 1667 | 1667 | 1588 | 1706 | 1555 | 1723 | 1525 | 1737 | 1475 | 1763 |
| 1.5 | 2500 | 2500 | 2322 | 2589 | 2248 | 2626 | 2182 | 2659 | 2069 | 2716 |
| 2.0 | 3667 | 3667 | 3351 | 3825 | 3219 | 3890 | 3101 | 3949 | 2900 | 4050 |

In order to better understand the contour patterns of $f_i/f_{BM}$, it is useful to first present results for the relaxation collision model. For this collision model, contours of $f_i/f_{BM}$ in the principal $c_x - c_\parallel$ velocity plane are shown in Fig. 7 for the same set of parameters that led to the $f_i/f_M$ contours shown in Fig. 6. A comparison of corresponding contour patterns reveals several important differences. First, the $f_i/f_{BM}$ contours are straight lines, while the $f_i/f_M$ contours form closed loops. To understand this difference we note that for the relaxation model the effect of a perpendicular electric field is felt only in perpendicular velocity planes; the ion distribution parallel to **B** is Maxwellian at the temperature of the neutral gas. This Maxwellian behaviour in the $c_\parallel$ direction is completely contained within the bi-Maxwellian part (weighting function) of our series expansion. As a consequence, $f_i/f_{BM}$ is independent of $c_\parallel$ and straight lines result when this ratio is plotted on a $c_\parallel - c_x$ velocity grid.

A comparison of Figs. 6 and 7 also indicates that, in general, the ratio $f_i/f_{BM}$ is closer to one than $f_i/f_M$, indicating that the ion velocity distribution is better approximated by a bi-Maxwellian than by an equivalent Maxwellian. However, the departures of $f_i$ from a bi-Maxwellian become significant for $D' \geq 1$, and the tendency of $f_i$ to take a toroidal shape is reflected (in Fig. 7) by the depletion (relative to $f_{BM}$) of ions near the origin and by the enhancements near $c_x = \pm 1.5 v_{T_i}$.

With regard to the question of convergence, the values of $f_i/f_{BM}$ shown in Fig. 7 indicate that our series converges for all parallel ion velocities and for a range of perpendicular ion velocities that depends on the strength of the electric field. The perpendicular velocity range is $|c_x| \lesssim 2.75 v_{T_i}$ for $D' = 0.5$, $|c_x| \lesssim 2.5 v_{T_i}$ for $D' = 1$, and $|c_x| \lesssim 2.25 v_{T_i}$ for $D' = 1.5$. Consequently, for all three electric field strengths our series is capable of describing the bulk of the ions.

In Fig. 8 we present contours of $f_i/f_{BM}$ in the principal $c_x - c_\parallel$ velocity plane for the resonant charge exchange collision model. Relative to the bi-Maxwellian, there is a depletion of ions near the origin and enhancements near $c_x = \pm 1.5 v_{T_i}$, which is similar to the result obtained for the relaxation model. However, the depletion and enhancements are not quite as large as those obtained for the relaxation model. In contrast to the relaxation model results, enhancements also occur along the $c_\parallel$-axis for both large negative and large positive values of $c_\parallel$. Furthermore, it is readily apparent that the contours of $f_i/f_{BM}$ for resonant charge exchange are not straight lines, as they are for the relaxation

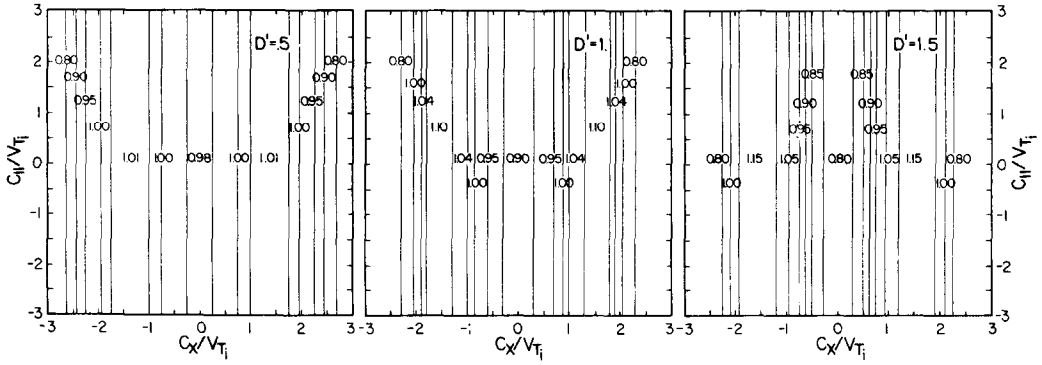


FIG. 7. CONTOURS OF $f_i/f_{BM}$ IN THE PRINCIPAL $c_x - c_\parallel$ VELOCITY PLANE FOR THE RELAXATION COLLISION MODEL.

In this figure, $D' = D/v_{T_n}$, $D = E_\perp c/B$, $v_{T_n} = (2kT_n/m_n)^{1/2}$ and $v_{T_i} = (2kT_i/m_i)^{1/2}$.

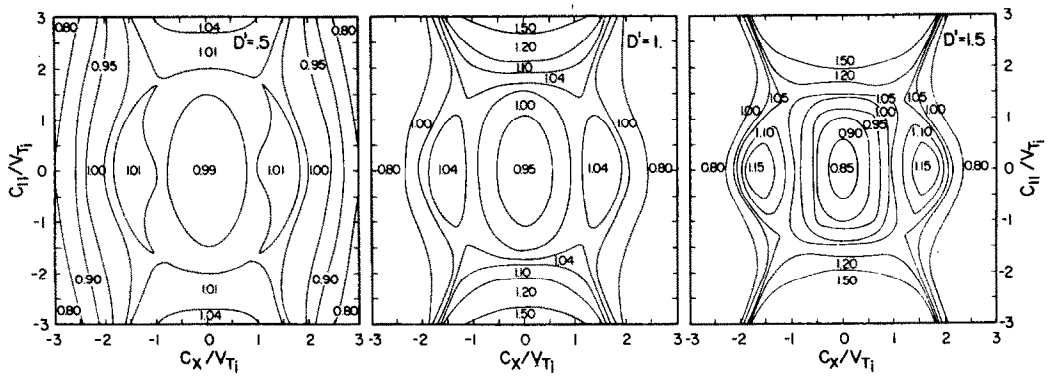


FIG. 8. CONTOURS OF $f_i/f_{BM}$ IN THE PRINCIPAL $c_x$–$c_\parallel$ VELOCITY PLANE FOR THE RESONANT CHARGE EXCHANGE COLLISION MODEL.

In this figure, $D' = D/v_{T_n}$, $D = E_\perp c/B$, $v_{T_n} = (2kT_n/m_n)^{1/2}$ and $v_{T_i} = (2kT_i/m_i)^{1/2}$.

model. This difference results because the resonant charge exchange model, unlike the relaxation model, is not a pure back-scattering model, and therefore, the effects of a perpendicular electric field are not confined to perpendicular velocity planes, but are felt in parallel planes as well.

Overall, the departures of $f_i$ from the bi-Maxwellian are smaller for resonant charge exchange than for the relaxation model. Furthermore, the departures of $f_i$ from the equivalent Maxwellian are also smaller for resonant charge exchange, since the perpendicular–parallel temperature difference is smaller. This behavior is a direct consequence of the fact that resonant charge exchange collisions are more isotropic than relaxation model collisions.

In Figs. 9–11 we present contours of $f_i/f_{BM}$ in the principal $c_x$–$c_\parallel$ velocity plane for the polarization collision model and three ion–neutral mass ratios ($\frac{1}{2}$, 1, 2). The polarization model results for $m_i/m_n = 1$ can be directly compared to both the resonant charge exchange and the relaxation model results, since a mass ratio of unity is implied in both of these models. A comparison of corresponding contours indicates that the polarization pattern is distinctly different from either the resonant charge exchange or the relaxation model patterns, although certain features are similar. Relative to the bi-Maxwellian, $f_i$ is depressed near the origin and enhanced near $c_x = \pm 1.5 v_{T_i}$, which is in agreement with the behaviour obtained for both the resonant charge exchange and relaxation models. Also, there are enhancements in $f_i$ close to the $c_\parallel$-axis for both large positive and large negative values of $c_\parallel$, in agreement with the resonant charge exchange model results. However, these enhancements are confined to a much smaller region of velocity space for the polarization model than for the resonant charge exchange model.

In general, the departures of $f_i$ from both the bi-Maxwellian and the equivalent Maxwellian are smaller for the polarization model than for either the resonant charge exchange or relaxation models,

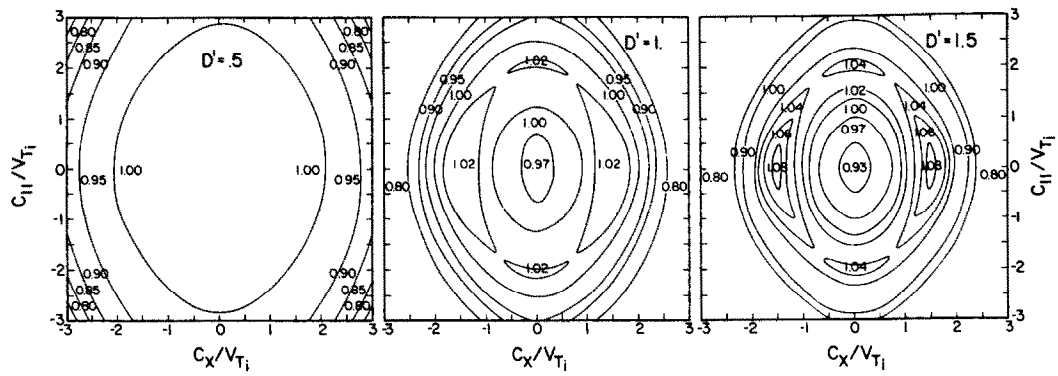


FIG. 9. CONTOURS OF $f_i/f_{BM}$ IN THE PRINCIPAL $c_x$–$c_\parallel$ VELOCITY PLANE FOR THE POLARIZATION COLLISION MODEL AND $m_i/m_n = \frac{1}{2}$.

In this figure, $D' = D/v_{T_n}$, $D = E_\perp c/B$, $v_{T_n} = (2kT_n/m_n)^{1/2}$ and $v_{T_i} = (2kT_i/m_i)^{1/2}$.

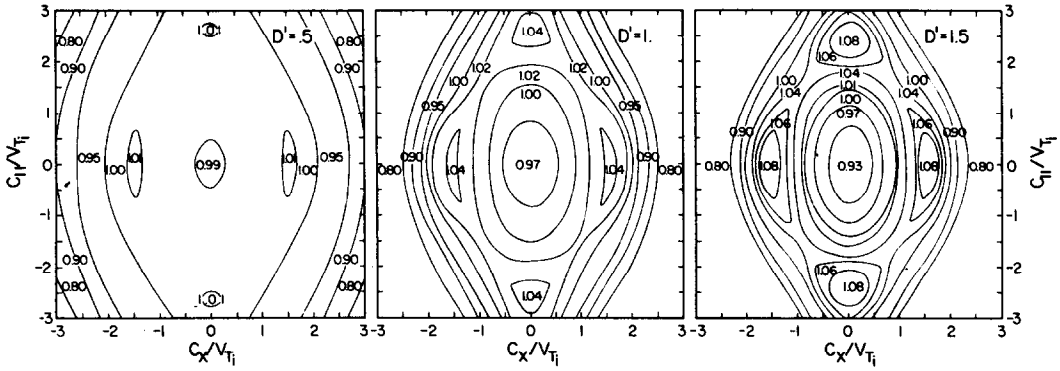


FIG. 10. CONTOURS OF $f_i/f_{BM}$ IN THE PRINCIPAL $c_x$–$c_\parallel$ VELOCITY PLANE FOR THE POLARIZATION COLLISION MODEL AND $m_i/m_n = 1$.
In this figure, $D' = D/v_{T_n}$, $D = E_\perp c/B$, $v_{T_n} = (2kT_n/m_n)^{1/2}$ and $v_{T_i} = (2kT_i/m_i)^{1/2}$.

which indicates that the polarization scattering mechanism is more isotropic than the other scattering mechanisms.

The effect on the ion velocity distribution of different ion-neutral mass ratios can be seen by comparing Figs. 9–11. For the three mass ratios considered ($\frac{1}{2}$, 1, 2), the contour patterns for a given value of $D'$ are very similar. In general, as the ion-neutral mass ratio increases from $\frac{1}{2}$ to 2, the departures of $f_i$ from the bi-Maxwellian increase. Likewise, the departures of $f_i$ from the equivalent Maxwellian increase as $m_i/m_n$ is increased, since increases in $m_i/m_n$ lead to greater perpendicular–parallel temperature differences (see Table 5).

In Fig. 12 we present contours of $f_i/f_{BM}$ in the principal $c_x$–$c_\parallel$ velocity plane for the forward scattering model. Although this collision model is not a physically realistic model, its scattering properties are opposite from that of the relaxation model, and, therefore, between the two models we are able to cover the complete range of classical scattering behaviour for elastic ion–neutral interactions. The most striking feature of the forward scattering model is that the ion velocity distribution is approximately bi-Maxwellian even for relatively large electric field strengths. In fact, in order to obtain values of $f_i/f_{BM}$ that are the same order of magnitude as those shown in our previous contour plots, it was necessary to set $D' = 1.5$, 2.5, and 3.5, instead of 0.5, 1, and 1.5.

The forward scattering model differs from the other scattering models in two important ways. First, as discussed earlier, $T_{i\parallel} > T_{i\perp}$ for the forward scattering model, while the reverse is true for the other scattering models. Also, relative to the bi-Maxwellian, $f_i$ is enhanced near the origin and depressed near $c_x = \pm 1.5 v_{T_i}$ and near $c_\parallel = \pm 2 v_{T_i}$ which is in contrast to the behaviour obtained for the other scattering models.

Finally, we note that the ion velocity distribution takes simple forms in the asymptotic limits of very small and very large ion-neutral mass ratios. In the

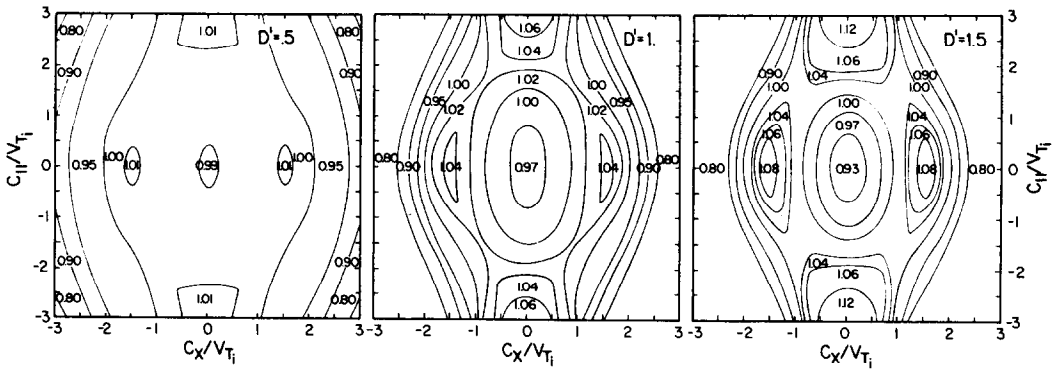


FIG. 11. CONTOURS OF $f_i/f_{BM}$ IN THE PRINCIPAL $c_x$–$c_\parallel$ VELOCITY PLANE FOR THE POLARIZATION COLLISION MODEL AND $m_i/m_n = 2$.
In this figure, $D' = D/v_{T_n}$, $D = E_\perp c/B$, $v_{T_n} = (2kT_n/m_n)^{1/2}$ and $v_{T_i} = (2kT_i/m_i)^{1/2}$.

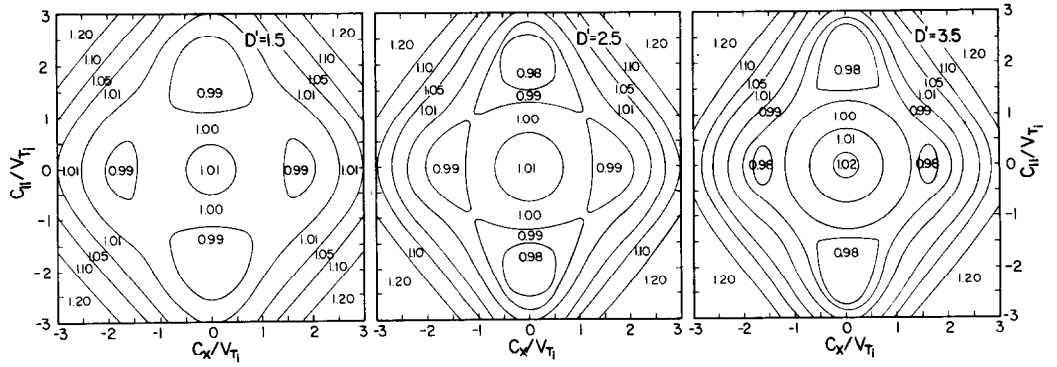


FIG. 12. CONTOURS OF $f_i/f_{BM}$ IN THE PRINCIPAL $c_x$–$c_{\parallel}$ VELOCITY PLANE FOR THE FORWARD SCATTERING MODEL AND $m_i/m_n = 1$.
In this figure, $D' = D/v_{T_n}$, $D = E_{\perp}c/B$, $v_{T_n} = (2kT_n/m_n)^{1/2}$ and $v_{T_i} = (2kT_i/m_i)^{1/2}$.

limit $m_i/m_n \to 0$, the ion velocity distribution is Maxwellian for all collision models and arbitrary electric field strengths. In the opposite limit of $m_i/m_n \to \infty$, the ion velocity distribution is a pure bi-Maxwellian, again for all collision models and arbitrary electric field strengths. In addition, for a given electric field strength, the difference between $T_{i\parallel}$ and $T_{i\perp}$ is greater for $m_i/m_n \to \infty$ than for any other value of $m_i/m_n$. However, as shown above, for finite values of $m_i/m_n$ deviations from a bi-Maxwellian are appreciable and should be considered in auroral studies involving ion velocity distributions.

## 5. SUMMARY AND CONCLUSIONS

We have calculated ion velocity distributions for a weakly-ionized plasma that has been subjected to crossed electric and magnetic fields. The appropriate Boltzmann equation has been solved by expanding the ion velocity distribution function in a generalized orthogonal polynomial series about a bi-Maxwellian weight factor. With this method of solution, we have been able to obtain reliable expressions for the ion velocity distribution function for a range of ion–neutral scattering mechanisms and for convection electric field strengths as large as 90 mV m$^{-1}$.

As far as ion-neutral scattering mechanisms are concerned, our main emphasis has been devoted to a polarization-hard core (12-4) interaction potential, which approximately yields a velocity independent ion–neutral collision frequency. For this collision model, we have considered a range of ion-neutral mass ratios ($m_i/m_n = 0, \frac{1}{2}, 1, 2, \infty$). The mass ratios of $\frac{1}{2}$, 1 and 2 cover the important ion-neutral collision combinations at $E$ and $F$-region altitudes, while the asymptotic limits $m_i/m_n \to 0$ and $\infty$ are useful since they provide information on the ion-neutral scattering behaviour in the limits of very light and very heavy ions, respectively. In addition to the polarization model, we have also considered a resonant charge exchange model as well as other collision models such as the relaxation model (back-scattering) and the forward scattering model. These latter collision models were useful, since with these models we have been able to cover the complete range of classical scattering behaviour for elastic ion-neutral interactions.

For all collision models, we have found that to lowest order the ion velocity distribution is bi-Maxwellian, with different ion temperatures parallel and perpendicular to the geomagnetic field. In general, the perpendicular–parallel temperature difference depends on the ion-neutral collision model and mass ratio as well as on the magnitude of the convection electric field. For the physically realistic polarization and resonant charge exchange collision models, $T_{i\perp} > T_{i\parallel}$, indicating that for these models the ion velocity distribution decreases more slowly in the perpendicular velocity plane with increasing ion velocity than in the parallel velocity plane. Typical perpendicular and parallel temperatures as a function of convection electric field have been presented in Tables 4 and 5 for different ion-neutral collision models and mass ratios.

Although the bi-Maxwellian form may be useful for certain auroral studies, we have found that departures of the ion velocity distribution from the zeroth-order bi-Maxwellian become significant when the ion convection velocity approaches (or exceeds) the neutral thermal speed. Furthermore, for a given convection electric field the departures generally increase as the ion-neutral scattering mechanism varies from forward scattering to back

scattering. For the polarization and resonant charge exchange collision models, the departures from the zeroth-order bi-Maxwellian, which peaks at the ion $\mathbf{E}_\perp \times \mathbf{B}$ drift velocity, are such as to decrease the number of ions at the peak and to increase the number in both the perpendicular and parallel velocity planes at ion speeds between about $1.5-2v_{T_i}$, where $v_{T_i}=(2kT_i/m_i)^{1/2}$ is the ion thermal speed and $T_i=(T_{i\parallel}+2T_{i\perp})/3$ is the ion temperature.

The ion velocity distributions that we have obtained for resonant charge exchange collisions are not as anisotropic as those obtained from the relaxation collision model. Consequently, the instability threshold of the $O^+$ velocity distribution in the auroral ionosphere is likely to be considerably higher than the estimate of 40 mV m$^{-1}$ given by Ott and Farley (1975). Recent measurements of ion velocity distributions from the retarding potential analyzer on the Atmosphere Explorer-C satellite suggest an $O^+$ instability threshold as high as 80 mV m$^{-1}$ or greater (St-Maurice *et al.*, 1976). We also note that the instability threshold of the $NO^+$ velocity distribution is higher than for $O^+$ ions, since polarization interactions lead to more isotropic velocity distributions than resonant charge exchange interactions.

Finally, we note that Wannier (1953) has studied the motion of ions in a weakly-ionized plasma subjected to a uniform electric field and no magnetic field. He obtained different ion temperatures parallel and perpendicular to the electric field, and his expressions for these temperatures are similar in form to our zeroth-order bi-Maxwellian temperatures (33) and (34). It therefore appears that our method of solution of Boltzmann's equation may be useful for ion mobility studies.

*Acknowledgements*—This research was supported, in part, by NSF Grant ATM74-21090A02 at the University of Michigan and, in part, by NSF Grant DES74-22343 at the University of California, San Diego.

## REFERENCES

Allis, W. P. (1956). Motions of ions and electrons. *Handbuch der Physik* **21,** 383–444.

Banks, P. M. (1966). Collision frequencies and energy transfer, ions. *Planet. Space Sci.* **14,** 1105–1122.

Banks, P. M. and Kockarts, G. (1973). *Aeronomy.* Academic Press, New York.

Chapman, S. and Cowling, T. G. (1970). *The Mathematical Theory of Non-Uniform Gases.* Cambridge University Press, London.

Cole, K. D. (1971). Atmospheric excitation and ionization by ions in strong auroral and man-made electric fields. *J. atmos. terr. Phys.* **33,** 1241–1249.

Dalgarno, A. (1958). The mobilities of ions in their parent gases. *Phil. Trans. R. Soc.* (A)**250,** 426–439.

Dalgarno, A., McDowell, M. R. C. and Williams, A. (1958). The mobilities of ions in unlike gases. *Phil. Trans. R. Soc.* (A)**250,** 411–425.

Grad, H. (1958). Principles of the kinetic theory of gases. *Handbuch der Physik XII,* 205–294.

Hassé, H. R. and Cook, W. R. (1929). The determination of molecular forces from the viscosity of a gas. *Proc. R. Soc. London* **125,** 196–221.

Hassé, H. R. and Cook, W. R. (1931). The calculation of the mobility of monomolecular ions. *Phil. Mag.* **12,** 554–566.

Langevin, P. (1905). Une formule fondamentale de théorie cinétique. *Ann. Chim. Phys.* **5,** 245–288.

Mason, E. A. (1970). Estimated ion mobilities for some air constituents. *Planet. Space Sci.* **18,** 137–144.

Mason, E. A. and Schamp, H. W. (1958). Mobility of gaseous ions in weak electric fields. *Ann. Phys.* **4,** 233–270.

Mason, E. A., Vanderslice, J. T. and Yos, J. M. (1959). Transport properties of high-temperature multicomponent gas mixtures. *Phys. Fluids* **2,** 688–694.

McDaniel, E. W. and Mason, E. A. (1973). *The Mobility and Diffusion of Ions in Gases.* Wiley, New York.

McFarland, M., Albritton, D. L., Fehsenfeld, F. C., Ferguson, E. E. and Schmeltekopf, A. L. (1973). Flow-drift technique for ion mobility and ion–molecule reaction rate constant measurements. II. Positive ion reactions of $N^+$, $O^+$, and $N_2^+$ with $O_2$ and $O^+$ with $N_2$ from thermal to ~2 eV. *J. Chem. Phys.* **59,** 6620–6628.

Ott, E. and Farley, D. T. (1975). Micro-instabilities and the production of short wavelength irregularities in the auroral *F* region. *J. geophys. Res.* **80,** 4599–4602.

Schunk, R. W., Banks, P. M. and Raitt, W. J. (1976). Effects of electric fields and other processes upon the nighttime high latitude *F*-layer. *J. geophys. Res.* **81,** 3271–3282.

Schunk, R. W., Raitt, W. J. and Banks, P. M. (1975). Effect of electric fields on the daytime high-latitude *E*- and *F*-regions. *J. geophys. Res.* **80,** 3121–3130.

Schunk, R. W. and Walker, J. C. G. (1972). Ion velocity distributions in the auroral ionosphere. *Planet. Space Sci.* **20,** 2175–2191.

St-Maurice, J.-P. (1975). Ion velocity distributions in the auroral ionosphere. Ph.D. Thesis. Yale University, New Haven, Connecticut.

St-Maurice, J.-P., Hanson, W. B. and Walker, J. C. G. (1976). Retarding potential analyzer measurements of the effect of ion–neutral collisions on the ion velocity distribution in the auroral ionosphere. Submitted to the *J. geophys. Res.*

St-Maurice, J.-P. and Schunk, R. W. (1973). Auroral ion velocity distributions using a relaxation model. *Planet. Space Sci.* **21,** 1115–1130.

St-Maurice, J.-P. and Schunk, R. W. (1974). Behaviour of ion velocity distributions for a simple collision model. *Planet. Space Sci.* **22,** 1–18.

St-Maurice, J.-P. and Schunk, R. W. (1976). Use of generalized orthogonal polynomial solutions of Boltzmann's equation in certain aeronomy problems: auroral ion velocity distributions. *J. geophys. Res.* **81,** 2145–2154.

Swift, D. W. (1975). The effect of electric fields and ion–neutral collisions on Thomson scatter spectra. *J. geophys. Res.* **80,** 4380–4382.

Wannier, G. H. (1953). Motion of gaseous ions in strong electric fields. *Bell System Tech. J.* **32,** 170–254.
Wannier, G. H. (1970). On an anomaly in the mobility of gaseous ions. *Bell System Tech. J.* **49,** 343–354.

## APPENDIX A

*Hermite polynomials*

The Hermite polynomials, $H_m(X)$, are orthogonal with respect to the weight function $e^{-X^2}$ over the range $-\infty < X < \infty$. The generating function for these polynomials is

$$\exp(-t^2+2tX) = \sum_{m=0}^{\infty} \frac{t^m}{m!} H_m(X). \tag{A1}$$

In particular, the first few Hermite polynomials are

$$H_0(X) = 1 \tag{A2}$$
$$H_1(X) = 2X \tag{A3}$$
$$H_2(X) = 4X^2 - 2 \tag{A4}$$
$$H_3(X) = 8X^3 - 12X \tag{A5}$$
$$H_4(X) = 16X^4 - 48X^2 + 12 \tag{A6}$$

These polynomials are connected by the orthogonality relation

$$\int_{-\infty}^{\infty} dX\, e^{-X^2} H_m(X) H_p(X) = \delta_{mp} 2^m m! \sqrt{\pi}. \tag{A7}$$

*Associated Laguerre polynomials*

The associated Laguerre polynomials, $L_n^0(X)$, are orthogonal with respect to the weight function $e^{-X}$ over the range $0 \le X < \infty$. The generating function for these polynomials is

$$\frac{\exp(-Xt/(1-t))}{(1-t)} = \sum_{n=0}^{\infty} \frac{t^n}{\Gamma(n+1)} L_n^0(X). \tag{A8}$$

In particular, the first few polynomials are

$$L_0^0(X) = 1 \tag{A9}$$
$$L_1^0(X) = 1 - X \tag{A10}$$
$$L_2^0(X) = 2 - 4X + X^2 \tag{A11}$$
$$L_3^0(X) = 6 - 18X + 9X^2 - X^3 \tag{A12}$$
$$L_4^0(X) = 24 - 96X + 72X^2 - 16X^3 + X^4. \tag{A13}$$

These polynomials are connected by the orthogonality relation

$$\int_0^{\infty} dX e^{-X} L_q^0(X) L_n^0(X) = \delta_{qn} [\Gamma(n+1)]^2, \tag{A14}$$

where $\Gamma(y)$ is the Gamma function (Hildebrand, 1964).

## APPENDIX B

Moments of Boltzmann's equation can be obtained by multiplying equations (9) and (10) by $\Phi_i = \Phi_i(\mathbf{c}_i)$ and then integrating over velocity space. From equation (9) we have

$$\int d\mathbf{c}_i \Phi_i \frac{\partial f_i^{(0)}}{\partial \alpha} = 0 \tag{B1}$$

or

$$\int d\mathbf{c}_i f_i^{(0)} \frac{\partial \Phi_i}{\partial \alpha} = 0, \tag{B2}$$

where the second expression is obtained by integrating by parts and by using the fact that $\Phi_i f_i^{(0)}$ is periodic in $\alpha$ with a period of $2\pi$. The same procedure applied to equation (10) yields

$$-\Omega_i \int d\mathbf{c}_i \Phi_i \frac{\partial f_i^{(1)}}{\partial \alpha} = \int d\mathbf{c}_i\, d\mathbf{v}_n\, d\Omega g_{in} \sigma_{in}(g_{in}, \theta)[\bar{f}_i^{(0)} \bar{f}_n - f_i^{(0)} f_n] \Phi_i \tag{B3}$$

or

$$\Omega_i \int d\mathbf{c}_i f_i^{(1)} \frac{\partial \Phi_i}{\partial \alpha} = \int d\mathbf{c}_i\, d\mathbf{v}_n\, d\Omega g_{in} \sigma_{in}(g_{in}, \theta) f_i^{(0)} f_n [\bar{\Phi}_i - \Phi_i], \tag{B4}$$

where, as before, the left-hand side of the second expression follows from an integration by parts, while the right-hand side follows from the reversibility of elastic collisions (cf. Allis, 1956).

The collision integral is evaluated by introducing both the center-of-mass velocity, $\mathbf{V}_c$, and the relative velocity, $\mathbf{g}_{in}$, of the colliding particles $i$ and $n$,

$$\mathbf{V}_c = \langle \mathbf{v}_i \rangle + \frac{m_i \mathbf{c}_i + m_n \mathbf{c}_n}{m_i + m_n} \equiv \mathbf{V} + \langle \mathbf{v}_i \rangle \tag{B5}$$
$$\mathbf{g}_{in} = \mathbf{c}_i - \mathbf{c}_n, \tag{B6}$$

where

$$\mathbf{c}_i = \mathbf{v}_i - \langle \mathbf{v}_i \rangle \tag{B7}$$
$$\mathbf{c}_n \equiv \mathbf{v}_n - \langle \mathbf{v}_i \rangle. \tag{B8}$$

and where the velocity $\mathbf{V}$ is introduced for convenience. From equations (B5) and (B6), we have

$$\mathbf{c}_i = \mathbf{V} + \frac{m_n}{m_i + m_n} \mathbf{g}_{in} \tag{B9}$$

$$\bar{\mathbf{c}}_i = \mathbf{V} + \frac{m_n}{m_i + m_n} \bar{\mathbf{g}}_{in}, \tag{B10}$$

where the velocity $\mathbf{V}$ is not changed in a collision.

The quantity $(\bar{\Phi}_i - \Phi_i)$ can now be obtained from equations (B9) and (B10). In addition to the trivial value of $\Phi_i = 1$, in the present study it is necessary to consider two values of $\Phi_i$; $\Phi_i = \mathbf{c}_i \mathbf{c}_i$ and $\Phi_i = \mathbf{c}_i \mathbf{c}_i \mathbf{c}_i \mathbf{c}_i$. For these values of $\Phi_i$, equations (B9) and (B10) yield

$$[\bar{c}_\alpha \bar{c}_\beta - c_\alpha c_\beta] = M_n^2 [\bar{g}_\alpha \bar{g}_\beta - g_\alpha g_\beta] + M_n [V_\alpha (\bar{g}_\beta - g_\beta) + (\bar{g}_\alpha - g_\alpha) V_\beta] \tag{B11}$$

$$\begin{aligned}[\bar{c}_\alpha \bar{c}_\beta \bar{c}_\gamma \bar{c}_\varepsilon - c_\alpha c_\beta c_\gamma c_\varepsilon] = {} & M_n^4 [\bar{g}_\alpha \bar{g}_\beta \bar{g}_\gamma \bar{g}_\varepsilon - g_\alpha g_\beta g_\gamma g_\varepsilon] \\ & + M_n^3 \{(\bar{g}_\alpha \bar{g}_\beta \bar{g}_\gamma - g_\alpha g_\beta g_\gamma) V_\varepsilon + (\bar{g}_\alpha \bar{g}_\beta \bar{g}_\varepsilon - g_\alpha g_\beta g_\varepsilon) V_\gamma \\ & + (\bar{g}_\alpha \bar{g}_\gamma \bar{g}_\varepsilon - g_\alpha g_\gamma g_\varepsilon) V_\beta + (\bar{g}_\beta \bar{g}_\gamma \bar{g}_\varepsilon - g_\beta g_\gamma g_\varepsilon) V_\alpha \} \\ & + M_n^2 \{(\bar{g}_\alpha \bar{g}_\beta - g_\alpha g_\beta) V_\gamma V_\varepsilon + (\bar{g}_\alpha \bar{g}_\gamma - g_\alpha g_\gamma) V_\beta V_\varepsilon \\ & + (\bar{g}_\alpha \bar{g}_\varepsilon - g_\alpha g_\varepsilon) V_\beta V_\gamma + (\bar{g}_\beta \bar{g}_\gamma - g_\beta g_\gamma) V_\alpha V_\varepsilon \\ & + (\bar{g}_\beta \bar{g}_\varepsilon - g_\beta g_\varepsilon) V_\alpha V_\gamma + (\bar{g}_\gamma \bar{g}_\varepsilon - g_\gamma g_\varepsilon) V_\alpha V_\beta \} \\ & + M_n \{(\bar{g}_\alpha - g_\alpha) V_\beta V_\gamma V_\varepsilon + (\bar{g}_\beta - g_\beta) V_\alpha V_\gamma V_\varepsilon \\ & + (\bar{g}_\gamma - g_\gamma) V_\alpha V_\beta V_\varepsilon + (\bar{g}_\varepsilon - g_\varepsilon) V_\alpha V_\beta V_\gamma \},\end{aligned} \tag{B12}$$

where

$$M_n = m_n/(m_i + m_n). \tag{B13}$$

In equations (B11), (B12) and all subsequent equations, we drop the subscript "$i$" from $\mathbf{c}_i$ and the subscripts "$in$" from $\mathbf{g}_{in}$ for simplicity. Furthermore, we introduce index notation for the tensors through the use of Greek subscripts.

When evaluating the collision integral, it is convenient to first integrate over the solid angle $d\Omega = \sin\theta\, d\theta\, d\psi$. This can best be done by adopting a spherical coordinate system in the center-of-mass reference frame with the relative velocity $\mathbf{g}$ taken along the $\theta = 0$ axis. For the velocity terms appearing in equations (B11) and (B12), we need the following integrals:

$$\int d\Omega \sigma_{in}(g,\theta)(\bar{g}_\alpha - g_\alpha) = -g_\alpha Q_{in}^{(1)} \tag{B14}$$

$$\int d\Omega \sigma_{in}(g,\theta)(\bar{g}_\alpha \bar{g}_\beta - g_\alpha g_\beta) = \tfrac{1}{2}[g^2\,\delta_{\alpha\beta} - 3g_\alpha g_\beta] Q_{in}^{(2)} \tag{B15}$$

$$\begin{aligned}\int d\Omega \sigma_{in}(g,\theta)&(\bar{g}_\alpha \bar{g}_\beta \bar{g}_\gamma - g_\alpha g_\beta g_\gamma) \\ &= \tfrac{1}{2}[3Q_{in}^{(1)} - 5Q_{in}^{(3)}] g_\alpha g_\beta g_\gamma \\ &\quad + \tfrac{1}{2}[Q_{in}^{(3)} - Q_{in}^{(1)}] g^2[\delta_{\alpha\beta} g_\gamma + \delta_{\beta\gamma} g_\alpha + \delta_{\alpha\gamma} g_\beta]\end{aligned} \tag{B16}$$

$$\begin{aligned}\int d\Omega \sigma_{in}(g,\theta)&(\bar{g}_\alpha \bar{g}_\beta \bar{g}_\gamma \bar{g}_\varepsilon - g_\alpha g_\beta g_\gamma g_\varepsilon) \\ &= \tfrac{5}{8}[6Q_{in}^{(2)} - 7Q_{in}^{(4)}] g_\alpha g_\beta g_\gamma g_\varepsilon + \tfrac{1}{8}[5Q_{in}^{(4)} - 6Q_{in}^{(2)}] \\ &\quad \times g^2[\delta_{\alpha\beta} g_\gamma g_\varepsilon + \delta_{\gamma\varepsilon} g_\alpha g_\beta + \delta_{\alpha\gamma} g_\beta g_\varepsilon + \delta_{\beta\varepsilon} g_\alpha g_\gamma + \delta_{\beta\gamma} g_\alpha g_\varepsilon \\ &\qquad + \delta_{\alpha\varepsilon} g_\beta g_\gamma] \\ &\quad + \tfrac{1}{8}[2Q_{in}^{(2)} - Q_{in}^{(4)}] g^4[\delta_{\alpha\beta}\,\delta_{\gamma\varepsilon} + \delta_{\alpha\gamma}\,\delta_{\beta\varepsilon} + \delta_{\alpha\varepsilon}\,\delta_{\beta\gamma}],\end{aligned} \tag{B17}$$

where we used the fact that for elastic collisions $|\bar{\mathbf{g}}| = |\mathbf{g}|$. In equations (B14) to (B17), $\delta_{\alpha\beta}$ is the Kronecker delta and $Q_{in}^{(l)}$ is the scattering cross section,

$$Q_{in}^{(l)} = 2\pi \int_0^\pi (1 - \cos^l\theta)\sigma_{in}(g,\theta)\sin\theta\, d\theta. \tag{B18}$$

The integral of equations (B11) and (B12) over $d\Omega$ can be readily obtained with the aid of equations (B14) to (B17). The next step in evaluating the collision term in (B4) is to express $\mathbf{g}$ and $\mathbf{V}$ in terms of $\mathbf{c}_i$ and $\mathbf{v}_n$ using equations (B5), (B7) and (B8). Since we can assume that $gQ_{in}^{(l)}$ is independent of velocity, the remaining integrals over $d\mathbf{c}_i$ and $d\mathbf{v}_n$ can then be performed. With this procedure, the collision term in equation (B4) is expressed in terms of velocity moments of the zeroth-order ion distribution function $f_i^{(0)}$.

In the present investigation, we need moment equations for the following velocity moments: $\langle c_\parallel^2\rangle$, $\langle c_\perp^2\rangle$, $\langle c_\parallel^4\rangle$, $\langle c_\perp^4\rangle$, and $\langle c_\parallel^2 c_\perp^2\rangle$. Equations for these moments can be obtained from equations (B2) and (B4) by selecting the appropriate expression for $\Phi_i$ and by separating the components of these equations. For example, moment equations for $\langle c_\parallel^2\rangle$ and $\langle c_\perp^2\rangle$ can be obtained by setting $\Phi_i = \mathbf{cc}$, with $(\bar{\Phi}_i - \Phi_i)$ given by equation (B11). With this $\Phi_i$, equation (B2) indicates that the tensor $\langle\mathbf{cc}\rangle$ is diagonal and that the two perpendicular elements are equal. The diagonal elements $\langle c_\parallel^2\rangle$ and $\langle c_\perp^2\rangle$ are then obtained by respectively taking the scalar product of $\mathbf{e}_\parallel\mathbf{e}_\parallel$ and $(\mathbf{I} - \mathbf{e}_\parallel\mathbf{e}_\parallel)$ with equation (B4), where $\mathbf{e}_\parallel$ is a unit vector parallel to the magnetic field and $\mathbf{I}$ is the unit dyadic. With this procedure, we obtain

$$\langle c_\parallel^2\rangle = \frac{kT_n}{m_i} + \frac{1}{4}\frac{m_n}{m_i}\left(1 + \frac{m_n}{m_i}\right)\frac{Q_{in}^{(2)}}{Q_{in}^{(1)}} \times \left[1 + \frac{3}{4}\frac{m_n}{m_i}\frac{Q_{in}^{(2)}}{Q_{in}^{(1)}}\right]^{-1} D^2 \tag{B19}$$

$$\langle c_\perp^2\rangle = \frac{2kT_n}{m_i} + \frac{m_n}{m_i}\left[1 + \frac{1}{4}\left(2\frac{m_n}{m_i} - 1\right)\frac{Q_{in}^{(2)}}{Q_{in}^{(1)}}\right] \times \left[1 + \frac{3}{4}\frac{m_n}{m_i}\frac{Q_{in}^{(2)}}{Q_{in}^{(1)}}\right]^{-1} D^2. \tag{B20}$$

Equations (B19) and (B20) can now be used to obtain the parallel and perpendicular ion temperatures by setting $\langle c_\parallel^2\rangle = kT_{i\parallel}/m_i$ and $\langle c_\perp^2\rangle = 2kT_{i\perp}/m_i$;

$$T_{i\parallel} = T_n + \frac{1}{4}\left(1 + \frac{m_n}{m_i}\right)\frac{Q_{in}^{(2)}}{Q_{in}^{(1)}}\left[1 + \frac{3}{4}\frac{m_n}{m_i}\frac{Q_{in}^{(2)}}{Q_{in}^{(1)}}\right]^{-1}\frac{m_n D^2}{k} \tag{B21}$$

$$T_{i\perp} = T_n + \frac{1}{2}\left[1 + \frac{1}{4}\left(2\frac{m_n}{m_i} - 1\right)\frac{Q_{in}^{(2)}}{Q_{in}^{(1)}}\right] \times \left[1 + \frac{3}{4}\frac{m_n}{m_i}\frac{Q_{in}^{(2)}}{Q_{in}^{(1)}}\right]^{-1}\frac{m_n D^2}{k}. \tag{B22}$$

The procedure for obtaining moment equations for the fourth-order velocity moments $\langle c_\parallel^4\rangle$, $\langle c_\perp^4\rangle$ and $\langle c_\parallel^2 c_\perp^2\rangle$ is similar to that described above for the second-order velocity moments. Setting $\Phi_i = \mathbf{cccc}$, with $(\bar{\Phi}_i - \Phi_i)$ given by equation (B12), three equations for the three velocity moments can be obtained by respectively taking the scalar product of $\mathbf{e}_\parallel\mathbf{e}_\parallel\mathbf{e}_\parallel\mathbf{e}_\parallel$, $(\mathbf{I} - \mathbf{e}_\parallel\mathbf{e}_\parallel)(\mathbf{I} - \mathbf{e}_\parallel\mathbf{e}_\parallel)$ and $(\mathbf{I} - \mathbf{e}_\parallel\mathbf{e}_\parallel)\mathbf{e}_\parallel\mathbf{e}_\parallel$ with equation (B4). These equations have the form

$$\begin{aligned}&d_{j1}\langle c_\parallel^4\rangle + d_{j2}\langle c_\perp^4\rangle + d_{j3}\langle c_\parallel^2 c_\perp^2\rangle + d_{j4}\langle c_{n\parallel}^2\rangle\langle c_\perp^2\rangle \\ &\quad + d_{j5}\langle c_{n\parallel}^2\rangle\langle c_\parallel^2\rangle + d_{j6}\langle c_{n\perp}^2\rangle\langle c_\perp^2\rangle + d_{j7}\langle c_{n\perp}^2\rangle\langle c_\parallel^2\rangle \\ &\quad + d_{j8}\langle c_{n\parallel}^4\rangle + d_{j9}\langle c_{n\perp}^4\rangle + d_{j10}\langle c_{n\parallel}^2 c_{n\perp}^2\rangle = 0,\end{aligned} \tag{B23}$$

where

$$\langle c_{n\parallel}^2\rangle = \frac{kT_n}{m_n} \tag{B24}$$

$$\langle c_{n\perp}^2\rangle = \frac{2kT_n}{m_n} + D^2 \tag{B25}$$

$$\langle c_{n\parallel}^4\rangle = 3\left(\frac{kT_n}{m_n}\right)^2 \tag{B26}$$

$$\langle c_{n\perp}^4\rangle = 8\left(\frac{kT_n}{m_n}\right)^2 + 8\left(\frac{kT_n}{m_n}\right)D^2 + D^4 \tag{B27}$$

$$\langle c_{n\parallel}^2 c_{n\perp}^2\rangle = \frac{kT_n}{m_n}\left[\frac{2kT_n}{m_n} + D^2\right] \tag{B28}$$

and where $D$ is the magnitude of the ion $\mathbf{E}_\perp \times \mathbf{B}$ drift velocity and the $d$-coefficients are given in Appendix C. In equation (B23), the subscript $j = 1, 2, 3$ is used to identify the three equations.

For a given set of conditions, the three equations of the form (B23) can be inverted to obtain explicit values for $\langle c_\parallel^4\rangle$, $\langle c_\perp^4\rangle$ and $\langle c_\parallel^2 c_\perp^2\rangle$. These velocity moments can then be converted into $c_\parallel'$ and $c_\perp^*$ moments using equations (13) and (14) and the expressions for $T_{i\parallel}$ and $T_{i\perp}$ given by equations (B21) and (B22), respectively.

## APPENDIX C

The $d_{st}$ coefficients appearing in equation (B23) are given by:

$$d_{11} = -g[4M_i^3 M_n Q^{(1)} + 6M_i^2 M_n^2 Q^{(2)} + 4M_i M_n^3 Q^{(3)} + M_n^4 Q^{(4)}] \quad \text{(C1)}$$

$$d_{12} = \tfrac{3}{8} M_n^4 g[2Q^{(2)} - Q^{(4)}] \quad \text{(C2)}$$

$$d_{13} = M_n^2 g[-6M_i M_n [Q^{(1)} - Q^{(3)}] + 3(M_i^2 - M_n^2)Q^{(2)} + 3M_n^2 Q^{(4)}] \quad \text{(C3)}$$

$$d_{14} = 3M_n^4 g[2[Q^{(1)} - Q^{(3)}] + Q^{(4)}] \quad \text{(C4)}$$

$$d_{15} = -6M_n^2 g[2M_i(M_n - M_i)Q^{(1)} + (M_i^2 + M_n^2 - 4M_i M_n) \times Q^{(2)} + 2M_n(M_i - M_n)Q^{(3)} + M_n^2 Q^{(4)}] \quad \text{(C5)}$$

$$d_{16} = 4d_{12} \quad \text{(C6)}$$

$$d_{17} = d_{13} \quad \text{(C7)}$$

$$d_{18} = M_n^4 g[4Q^{(1)} - 6Q^{(2)} + 4Q^{(3)} - Q^{(4)}] \quad \text{(C8)}$$

$$d_{19} = d_{12} \quad \text{(C9)}$$

$$d_{1,10} = d_{14} \quad \text{(C10)}$$

$$d_{21} = M_n^4 [2Q^{(2)} - Q^{(4)}] \quad \text{(C11)}$$

$$d_{22} = -2M_i M_n (2M_i^2 + M_n^2) g Q^{(1)} - M_n^2 [5M_i^2 + \tfrac{1}{4} M_n^2] g Q^{(2)} - 2M_i M_n^3 g Q^{(3)} - \tfrac{3}{8} M_n^4 g Q^{(4)} \quad \text{(C12)}$$

$$d_{23} = M_n^2 g[-8M_i M_n [Q^{(1)} - Q^{(3)}] + (4M_i^2 - 2M_n^2)Q^{(2)} + 3M_n^2 Q^{(4)}] \quad \text{(C13)}$$

$$d_{24} = d_{23} \quad \text{(C14)}$$

$$d_{25} = 6d_{21} \quad \text{(C15)}$$

$$d_{26} = M_n^2 g[4(2M_i^2 - 3M_i M_n + M_n^2)Q^{(1)} - (2M_i^2 - 16M_i M_n + 3M_n^2)Q^{(2)} + 4M_n(M_n - M_i)Q^{(3)} - \tfrac{3}{2} M_n^2 Q^{(4)}] \quad \text{(C16)}$$

$$d_{27} = M_n^4 g[8[Q^{(1)} - Q^{(3)}] + 2Q^{(2)} + 3Q^{(4)}] \quad \text{(C17)}$$

$$d_{28} = d_{21} \quad \text{(C18)}$$

$$d_{29} = M_n^4 g[6Q^{(1)} - \tfrac{21}{4} Q^{(2)} + 2Q^{(3)} - \tfrac{3}{8} Q^{(4)}] \quad \text{(C19)}$$

$$d_{2,10} = d_{27} \quad \text{(C20)}$$

$$d_{31} = M_n^2 g[-2M_i M_n [Q^{(1)} - Q^{(3)}] + (M_i^2 - M_n^2)Q^{(2)} + M_n^2 Q^{(4)}] \quad \text{(C21)}$$

$$d_{32} = M_n^2 g[-M_i M_n [Q^{(1)} - Q^{(3)}] + (\tfrac{1}{2} M_i^2 - \tfrac{1}{4} M_n^2)Q^{(2)} + \tfrac{3}{8} M_n^2 Q^{(4)}] \quad \text{(C22)}$$

$$d_{33} = M_i M_n (-4M_i^2 + 3M_n^2) g Q^{(1)} - \tfrac{5}{2} M_n^2 [3M_i^2 - M_n^2] g Q^{(2)} - 7M_i M_n^3 g Q^{(3)} - 3M_n^4 g Q^{(4)} \quad \text{(C23)}$$

$$d_{34} = M_n^2 g[(2M_i^2 - M_n^2)Q^{(1)} + (-M_i^2 + 6M_i M_n + 2M_n^2)Q^{(2)} + M_n(3M_n - 4M_i)Q^{(3)} - 3M_n^2 Q^{(4)}] \quad \text{(C24)}$$

$$d_{35} = M_n^2 g[(M_i^2 - 4M_i M_n - 5M_n^2)Q^{(2)} + 6M_n(M_n - M_i)[Q^{(1)} - Q^{(3)}] + 6M_n^2 Q^{(4)}] \quad \text{(C25)}$$

$$d_{36} = M_n^2 g[2M_n(M_n - M_i)[Q^{(1)} - Q^{(3)}] + \tfrac{1}{2}(M_i^2 - 2M_i M_n - M_n^2)Q^{(2)} + \tfrac{3}{2} M_n^2 Q^{(4)}] \quad \text{(C26)}$$

$$d_{37} = M_n^2 g[(2M_i^2 - M_i M_n - 2M_n^2)Q^{(1)} - \tfrac{1}{2}(M_i^2 - 12M_i M_n - 3M_n^2)Q^{(2)} - M_n(3M_i - 4M_n)Q^{(3)} - 3M_n^2 Q^{(4)}] \quad \text{(C27)}$$

$$d_{38} = M_n^4 g[2[Q^{(1)} - Q^{(3)}] + Q^{(4)}] \quad \text{(C28)}$$

$$d_{39} = M_n^4 g[Q^{(1)} - Q^{(3)} + \tfrac{1}{4} Q^{(2)} + \tfrac{3}{8} Q^{(4)}] \quad \text{(C29)}$$

$$d_{3,10} = M_n^4 g[Q^{(1)} - 5Q^{(2)} + 7Q^{(3)} - 3Q^{(4)}], \quad \text{(C30)}$$

where for simplicity we have dropped the subscript "*in*" from the ion-neutral scattering cross sections and relative velocity. For pure polarization interactions, the quantity $gQ^{(l)}$ is independent of velocity for all values of $l$.